Elucidation of the Genetic and Developmental Mechanisms Underlying Choroid Fissure Closure

Lisa Tanya Tucker

University College London

Department of Cell and Developmental Biology

A thesis submitted for the degree of Master of Philosophy

Declaration

I, Lisa Tanya Tucker, confirm that the work presented in this thesis is my own. Where information has been derived from other sources, I confirm that this has been indicated in the thesis.

Impact Statement

In this work, I present new information on *lama1,* a gene involved in optic cup morphogenesis and, as a consequence, visual function. Zebrafish *lama1* mutants present coloboma, a congenital blindness disorder that, in humans, affects 1 in 5,000 births. By studying *lama1* mutants, I have been able to describe the effect of homozygosity of the *lama1 nl14* and *nl15* mutation on many aspects of optic cup morphogenesis as well as choroid fissure fusion and the impact on visual function. Despite disrupted *lama1* function being associated with numerous ocular phenotypes, coloboma has never been previously described. With this discovery, I have been able to add a new candidate gene to those already known to cause coloboma. With genomic screening becoming increasingly used in the diagnosis of genetic causes of coloboma, this gene can now be added to a potential genetic cause of coloboma when screening patients. Also, the *lama1* mutant phenotype is not fully penetrant and we can use the low penetrance of the coloboma phenotype in this mutant as a sensitised background to find additional risk factors for coloboma.

Moreover, I try to create a new tool to visualize choroid fissure cells. This will be a great benefit to the study of choroid fissure fusion, and, for instance, it will allow us to determine how choroid fissure cells behave in different genetic backgrounds in mutants with known coloboma phenotypes.

Acknowledgements

I have to say that this project hasn't been easy, and I wouldn't have got here without the help and support of many, many people. Brace yourselves, this is going to take a while…

My first thanks go to Steve and Gaia, my supervisors, for taking a chance on me 5 (!) years ago, for your continuous support and teaching me so much about the world of zebrafish and eye development.

To Paula, my secondary supervisor, who was always there when I just needed a friendly ear and for frequent discussions about this work.

To Yama, my tutor, for your help and guidance through this process.

To Debbie, for all the admin support when I have no idea what I'm doing.

To Alex Nechiporuk, for the coloboma lines.

To Richard Poole, for your help with processing the sequencing data.

To Eirinn, who also helped with the sequencing data but also for trying to teach me Python and assistance analysing the OKR data.

To Isaac Bianco, for allowing me to use your OKR set up, for help with the discussion of the data and for providing fish lines.

To Pedro and Paride who taught me how to embed fish for the OKR set up, you were very patient with my first failed attempts.

To Joanna, who helped me with the initial MatLab analysis of the OKR data, you worked your coding magic for me.

To Tom Hawkins, not only for your incredible chats, support and shared love of dachshunds but for teaching me the first steps of TEM.

To Mark Turmaine, our TEM wizard, for teaching me how to use the machine which I still think looks like something out of Doctor Who. You were so patient helping with everything from orientation, cutting, and helping me figure out what each grey 'blob' was.

To Gareth, for your advice and help with the CRISPR knock-in work and for your injection morning jokes.

To Chintan, for your help with 2-photon imaging and your thermostat control (even if I am always cold).

To the UCL fish facility staff, for your never-ending care of the fish and to Heather, who always reminds me when I'm behind with line regeneration.

To the guys from stores, for always smiling and being so kind, especially Michael who gives me chocolate when I'm having a bad day.

To Bill Andrews, for use of the central lab and always reminding me I'm a traitor (in rugby).

To the UCL Imaging staff, who constantly help when I have no idea what I'm doing on the confocal.

To Leo, you taught me so many things, you always involved me when you were trying new techniques and you always answered my stupid questions without ever telling me I was being stupid. Your support has never ended even when you've moved back to Chile, I will always appreciate everything you did for me.

It's not just the support with analysing data and learning new techniques that have made this project possible. I will inevitably forget someone in this list, but the first floor has never ceased to be a wonderful collaborative space to work and the lunch time chats have helped me get through the tough days…

To Claudia, for our shared stash of tea and for helping me learn the ropes of becoming a technician.

To Renato, for your endless support, your love of dancing and for trying but failing to find me a boyfriend in a gay bar, we had so many fun nights out and you made so many of my birthdays memorable!

To Maryam (MK), for all of your pep talks, encouraging my running and being my first commissioned cake customer. You were there to comfort me on such an awful day back in 2017, when my dear aunty had passed, and you pulled me aside and spoke such kind words. As a doctor I know that you have probably done the same thing for many patients' families, and you may not remember it, but I will forever remember the care you showed me in such a vulnerable moment.

To Shannon, for your warmth and kindness and your ever-inspiring chats. You and Camille have always been there to push me into seeing my potential and believing that I can achieve more.

To Nico, one of my lab brothers, for your energy, your knowing when I'm just having a bad day and need some help, and for allowing me to teach you the word 'faff'.

To Declan, my other lab brother, you have been so incredible in your never-ending support and your daily puns always make me smile.

To Ingrid, I will always remember one of our first conversations when you told me my aura was a mix of the colours yellow and 'percy pig' pink. I thought you were so weird but also wonderful. You taught me Estonian of which I still remember – aitäh!

To Sumi, you are quite possibly the kindest person in the world. You always ask me if I'm okay and you are always there if I ever need anything.

To Hande, for listening to my rants, advice on everything and general being there when I'm having a bad day.

To Joanna and Anya aka The Detectirinas, for the tea breaks, the birthday cakes, the chats about footy or any sport for that matter, the picking me up when I'm down, the daily laughs, the doggo videos, the detective work and the after-work Friday pub sessions. I couldn't have gotten through this without you.

To Liana, my desk buddy. Your Australian laid-back approach to everything was such a shock to my ever-awkward Britishness. You became such a good friend. Our trip to Oktoberfest, one of my absolute favourite weekends ever! Your spending Christmas with me and not complaining when I got the flu and could barely do anything. The amount of times we would be drunk after pub on Fridays and racing to catch the last tube home but always managing to get a McD's first. I have missed you so dearly since you went back home, and I know I have promised every year to visit you… 2020 might be the year! * due to covid-19 this will have to be postponed!

To Diz, our lab mother hen but my dear friend. You helped me when I felt like I had no one else. You always listened when I was having a bad day. I can't put into words how lucky I have been to have you.

It's safe to say the support outside the lab has also been unwavering…

To my Welsh lot aka The Alex and James Show, for the boozy brunches, the ridiculous cocktail happy hours, the rugby matches, the dinners and the telling me I'm being boring when I want to go home at 10pm. I'm sorry I haven't been around as much as I should have but I know you are always there for me when I'm in a state and don't know what to do.

To TPR, a very recent addition to my life. A running group like no other. I've only been a part of the family a few months but your help and kind words through balancing this writing and my marathon training have helped me so much. Your achievements inspire me daily. #TPRfamily #ForzaTPR #trustlloyd

And finally, to my family…

To my Grandparents, Archie and Ray, even though they have no clue what it is I actually do.

To my babas; Dory, Tinky, Lexi and dear Amby, my comfort blanket.

To my brother, Julian and sister-in-law, Emily. You have provided me with a place to escape on so many occasions. You always listen to my rants and moans and never complain, just provide me with a glass of wine and tell me it's okay. You are two of the best people I know. And Julian, I can't believe how lucky I am to have such a brilliant big brother.

To my Mum. Your continuous patience with me as I figure out what I'm doing with my life. You're never trying to stop me when I want to embark on another adventure. You make me feel better when I've had setbacks and end up crying down the phone. You have always believed in me, always pushed me, always put up with me when I'm being a drama queen. Your strength and resilience are inspiring, even though you don't realise it. You are superhuman and I am so grateful that you are my Mam.

And truly final now…

To my Dad. I can't even explain how much I miss you. I always wanted to be as clever as you. Everything I do is to make you proud.

Abstract

The choroid fissure is an opening in the ventral area of the developing optic cup that allows the hyaloid vasculature to enter and the retinal axons to exit the eye. Once this process has taken place, the choroid fissure will come together and fuse to form a continuous bilayered optic cup. If the choroid fissure fails to fuse, a permanent opening remains, giving a condition known as a coloboma. Coloboma is one of the most common congenital disorders in the world and can frequently cause blindness. However, the mechanisms underlying choroid fissure fusion are largely unknown. From mapping data, we discovered that disrupted function of *lama1* leads to coloboma in zebrafish. We analysed two alleles, one associated with a substitution of an amino acid in a highly conserved LamNT domain (*nl14)* and the other associated with a SNP that causes a premature stop codon (*nl15*). Using techniques such as *in situ* hybridisation, immunohistochemistry and optokinetic response (OKR), we were able to characterise the phenotype associated with mutations in *lama1*. The retina in mutant embryos develops as in wild-type siblings and no obvious disruption of the different layers, including the photoreceptors, was observed. However, there is a disrupted/reduced visual function in mutants compared to their siblings. This compromised visual function appears to be due to a combination of coloboma and disruption of the retinal projections. Therefore, disrupted function of *lama1* does cause coloboma and can be added to the already known list of genes associated with coloboma.

CONTENTS

TABLE OF FIGURES

LIST OF TABLES

Introduction

1.1 Anatomy of The Eye

Across vertebrate species, the anatomy, histology and circuitry of the eye is highly conserved (*Figure 1*; Bibliowicz, Tittle, & Gross, 2011a; Fadool & Dowling, 2008). The vertebrate eye develops from three different tissue types. The neuroectoderm will give rise to the retinal pigmented epithelium (RPE), neural retina (NR), and optic stalk (Fadool and Dowling, 2008). The periocular mesenchyme (POM) which is derived from neural crest and mesoderm, will form the connective tissue such as sclera and cornea (Bibliowicz, Rachel K. Tittle and Gross, 2011). The skin ectoderm which gives rise to the lens and subsequently the cornea (Fuhrmann, 2010; Bibliowicz, Rachel K. Tittle and Gross, 2011).

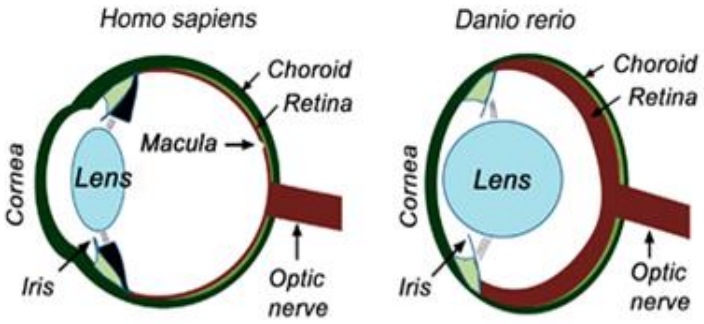

FIGURE 1 ANATOMY OF THE HUMAN VERSUS ZEBRAFISH

(A) The human eye consists of the lens, cornea and iris which allow the first entry for light in the visual pathway. The retina contains the macula and an external layer known as the choroid with signals passing to the brain via the optic nerve. (B) The zebrafish eye shows that the anatomy is conserved amongst species. It contains many of the same structures as the human eye such as cornea, iris, lens, retina, choroid and optic nerve. Image from Chhetri, Jacobson, & Gueven, 2014a.

1.2 Zebrafish as a model for eye development and visual function

Zebrafish have become a popular model choice in the past 20 years for the study of genetic mechanisms and development in health and disease. There are many reasons for this including their ease of maintenance and breeding (Richardson *et al.*, 2016). The adults take three to four months to be fully mature and able to reproduce. They produce large quantities (approximately 100-200) of eggs in one mating and are fertilized ex utero (Chhetri, Jacobson and Gueven, 2014). The major organs of the zebrafish develop and become fully functioning within two days and are transparent allowing for easy visualisation of organogenesis. As 70% of human genes have zebrafish orthologues and the zebrafish embryo is fertilized externally, it makes genetic manipulation easier and allows for high throughput genetic screening (Gestri, Link and Neuhauss, 2012; Chhetri, Jacobson and Gueven, 2014; Richardson *et al.*, 2016).

It is well known that the zebrafish is an excellent model system specifically for eye development due to similarities in gene expression, morphology, visual function and physiology to human eye development (Fadool and Dowling, 2008; Bibliowicz, Rachel K. Tittle and Gross, 2011; Gestri, Link and Neuhauss, 2012; Chhetri, Jacobson and Gueven, 2014; Richardson *et al.*, 2016). Furthermore, the retina is well differentiated by 72 hours post fertilisation (hpf) and visual function can be assessed at larva stage, as early as 4 days post fertilisation (dpf). Altogether, these features make the zebrafish an ideal model for the understanding of human eye development in health and disease (Bibliowicz, Rachel K. Tittle and Gross, 2011; Gestri, Link and Neuhauss, 2012; Chhetri, Jacobson and Gueven, 2014; Richardson *et al.*, 2016).

As my project is zebrafish based, in this introduction I will discuss eye development predominantly in the zebrafish with mention of other model systems where necessary.

1.3 Early Eye Development

1.3.1 Specification and Evagination of The Eye Field

Eye formation begins at late gastrulation as a single eye field in the anterior neural plate that is specified through various eye field transcription factors and signalling pathways (Cavodeassi, 2018). Once the eye field is specified, it will split from the midline into two lateral domains and will continue to evaginate from the diencephalon to form two separate optic vesicles (Ivanovitch 2013; Adler and Canto-Soler, 2007; Morris, 2011). Expression of eye field transcription factors (EFTFs); Rx, Pax6, Six3, Lhx2, Six6, ET, Otx2 and signalling pathways, such as; Fgfs, Wnt, BMP and Nodal are essential for this process (Zuber *et al.*, 2003; Wilson and Houart, 2004; Adler and Canto-Soler, 2007; Morris, 2011; Gestri, Link and Neuhauss, 2012). Moreover, mis-regulation of any of these factors will cause defects such as Anophthalmia (no eye), Microphthalmia (small eyes) or cyclopia (a persistent single eye field) (Adler and Canto-Soler, 2007; Morris, 2011).

Further, after the evagination of the optic vesicles, patterning of the optic vesicles requires differential expression of transcription factors as well as the influence of signalling pathways; Fgf, Bmp, Shh, and RA (Chow and Lang, 2001; Martínez-Morales, Rodrigo and Bovolenta, 2004; Lupo, Harris and Lewis, 2006; Adler and Canto-Soler, 2007; Fuhrmann, 2010). Simply, specification of the prospective optic stalk is predominantly determined by the expression of Pax2 and Vax; the prospective neural retina relies on Pax6, Lhx2, Rx and Chx10; the prospective RPE is determined by Mitf, Otx2 and Pax6. Moreover, boundaries are established between developing domains via Pax6 and Pax2 for NR and optic stalk, and Mitf and Chx10 for NR and RPE (Chow and Lang, 2001; Adler and Canto-Soler, 2007). Establishing the optic cup itself requires Lhx2, Pax6 and Hes1 (Chow and Lang, 2001; Canto-Soler and Adler, 2006; Adler and Canto-Soler, 2007).

1.4 Optic Cup Morphogenesis

1.4.1 Optic Cup and Lens formation

Once the optic vesicles are formed, they will fold asymmetrically, from dorsal to ventral to form two bilayered optic cups by 24hpf (Li, Joseph and Easter, 2000; Martinez-Morales and Wittbrodt, 2009). The bilayered structure comprises of the external retinal pigmented epithelium (RPE) which is derived from the dorsal region of the optic vesicle and the internal neural retina (NR) which is derived from the distal/ventral region of the optic vesicle (*Figure 2B;* Martinez-Morales & Wittbrodt, 2009; Sinn & Wittbrodt, 2013).

The formation of the optic cup involves a range of multiple complex tissue and cell arrangements (Bryan, Chien and Kwan, 2016; Cavodeassi, 2018; Buono *et al.*, 2020). First, the optic vesicle epithelium must fold along its anterior posterior axis (Martinez-Morales *et al.*, 2009). Prospective NR cells in the internal layer elongate along the apical-basal axis, the basal surface constricts but also maintain a wide apical surface, this results in the bending of the basal side of the NR (Martinez-Morales *et al.*, 2009; Cavodeassi, 2018; Buono *et al.*, 2020). NR formation is also accompanied by high proliferation rates which contributes to the bending of the optic cup (Kwan *et al.*, 2012). Moreover, future NR cells in the external layer elongate, undergo marked apical constriction and, display lamellipodial activity on their basal side (Cavodeassi, 2018). This results in the active migration at the optic cup rim of NR cells from the external to the internal layer of the developing optic cup in a process known as rim cell migration (*Figure 2A*; Sidhaye and Norden, 2017; Cavodeassi, 2018). In addition, basal constriction of the NR cells involves the basal localisation of focal adhesion complexes (Martinez-Morales *et al.*, 2009; Nicolá S-Pé Rez *et al.*, 2016). Tension along the epithelial sheet due to the linkage of the cells' cytoskeleton to extra cellular matrix (ECM), further results in the bending of the neuroepithelium (Martinez-Morales *et al.*, 2009; Nicolá S-Pé Rez *et al.*, 2016; Sidhaye and Norden, 2017; Cavodeassi, 2018; Patel and Sowden, 2019). The importance of the ECM in this part of optic cup formation is discussed in section 1.8.

In combination, the prospective RPE cells become flattened – the cells become shorter in the AB axis and expand their surface, further displacing surrounding cells to more distal regions (Cavodeassi, 2018). It is thought that the RPE helps optic cup morphogenesis by forming an outer shell around the 'softer' neural retina and the tension between the two layers as well as the apical constriction of rim cells induces optic cup formation (Moreno-Marmol, Cavodeassi and Bovolenta, 2018). This process is also thought to contribute to the active migration of cells through the rim into the ventral retina and forming the ventral neuroepithelium whilst at the dorsal pole, it remains static (Heermann *et al.*, 2015; Moreno-Marmol, Cavodeassi and Bovolenta, 2018).

Moreover, the dorsal to ventral folding of the optic cup leaves an opening in the ventral part of the eye known as the choroid or optic fissure (Fuhrmann, 2010; Bibliowicz, Rachel K. Tittle and Gross, 2011; Gestri, Link and Neuhauss, 2012; Bernstein *et al.*, 2018; Cavodeassi, 2018; Patel and Sowden, 2019). It is through this opening that the hyaloid vasculature enters and the retinal ganglion cell axons exit the eye (Bibliowicz, Rachel K. Tittle and Gross, 2011; Gestri, Link and Neuhauss, 2012; ALSomiry, Gregory-Evans and Gregory-Evans, 2019). As development of the eye continues, by 56hpf this opening will come together, fuse and give rise to continuous NR and RPE layers (*Figure 2D*; ALSomiry et al., 2019; Bibliowicz et al., 2011a; Gestri et al., 2012; Li et al., 2000).

As the optic cup is developing, the lens is also forming. The lens first develops as a lens placode in the surface ectoderm cells overlying the optic cup (Bibliowicz, Rachel K. Tittle and Gross, 2011). It invaginates along with the optic cup as the RPE and NR wrap around it. Invagination continues and appears coordinated between the retina and the lens until the lens placode delaminates and separates from the overlying ectoderm and becomes a fully formed solid lens mass (*Figure 2B-D*; Richardson et al., 2016).

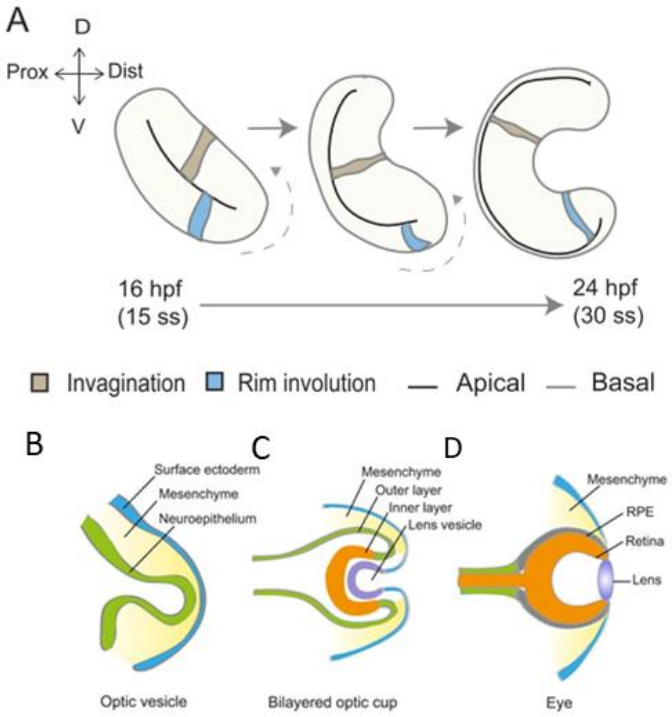

FIGURE 2 SCHEMATIC OF OPTIC CUP MORPHOGENESIS IN ZEBRAFISH

(A) A schematic of the cell movements during optic cup morphogenesis. The prospective neural retina cells that undergo invagination (grey) and prospective NR cells that undergo rim cell migration (blue). The dotted arrow shows the direction of rim cell involution. Image from Sidhaye and Norden, 2017. (B) The optic vesicle is formed by the neuroepithelium (green), mesenchyme (yellow) and surface ectoderm (blue). (C) The optic vesicle develops into a bi-layered optic cup. The surface ectoderm invaginates to form the lens vesicle (blue), the inner layer starts to develop and invaginate (orange) with the outer layer remaining (green). (D) The fully developed eye consisting of the lens (blue), neural retina (orange), retinal pigmented epithelium (RPE; dark blue). Image from Zhao, Wang, & Temple, 2017.

1.4.2 The differentiation of RPE and neural retina

The RPE initially proliferates to form a single layer of squamous cells that envelope the neural retina and is important for the full development of the eye including; growth, proper lamination and the differentiation of the photoreceptors (Fuhrmann, 2010). Once fully matured, the RPE cells are essential for the function, maintenance and protection of the photoreceptor layer (Bibliowicz, Rachel K Tittle and Gross, 2011; Gestri, Link and Neuhauss, 2012; Cechmanek and McFarlane, 2017; Moreno-Marmol, Cavodeassi and Bovolenta, 2018). The RPE cells contain specialized organelles – the

melanosomes, which accumulate pigment granules and are the crucial components in absorbing excess light entering the eye that would otherwise damage the photoreceptors (Moreno-Marmol, Cavodeassi and Bovolenta, 2018). The RPE cells also feature an apical membrane with protrusions that integrate with the closely located outer segment of the photoreceptors. This interaction is essential for adequate photoreceptor homeostasis including cyclic phagocytosis of the outer segment (Molday and Moritz, 2015). Furthermore, the RPE cells sit on the basement membrane separating the retina from the vasculature network of the choroid allowing for the regulation and recycling of nutrients and oxygen from the blood to the retina (Gestri, Link and Neuhauss, 2012; Moreno-Marmol, Cavodeassi and Bovolenta, 2018). This close interaction between RPE and photoreceptors allows them to be considered as a single functional unit. This is reflected in disorders affecting any one of these functions displaying progressive photoreceptor degeneration (Bibliowicz, Rachel K Tittle and Gross, 2011; Cechmanek and McFarlane, 2017; Moreno-Marmol, Cavodeassi and Bovolenta, 2018).

The neural retina is well differentiated by 72hpf in zebrafish and consists of three distinct layers, the ganglion cell layer (GCL), the inner nuclear layer (INL) and the outer nuclear layer (ONL) that are separated by two plexiform layers, consisting of six neural cell types and one glial (the Müller glia) (*Figure 3B*; Dhakal et al., 2015; Li et al., 2000). The GCL is the first to be established, in both humans and zebrafish. In zebrafish, the retinal ganglion cell (RGC) bodies are found in the GCL which further project axons via the optic stalk/optic nerve to their targets in the diencephalon and the optic tectum (Gestri, Link and Neuhauss, 2012; Dhakal *et al.*, 2015; Richardson *et al.*, 2016). The INL is occupied by the somata of the amacrine, bipolar and horizontal cells and Müller glial cell bodies (Gestri, Link and Neuhauss, 2012). The ONL contains the photoreceptors - highly polarised cells that are an essential unit for phototransduction and are further subdivided into two major classes; the rods and the cones (*Figure 3B*; Fadool & Dowling, 2008; Gestri et al., 2012; Molday & Moritz, 2015; Richardson et al., 2016). The rods are highly sensitive to light and therefore work under dim lighting conditions, whereas, the cones are responsive to bright light conditions and therefore are

responsible for colour vision and visual acuity (Molday and Moritz, 2015). The plexiform layers between these nuclear layers are where the synaptic connections are formed (Gestri, Link and Neuhauss, 2012; Richardson *et al.*, 2016).

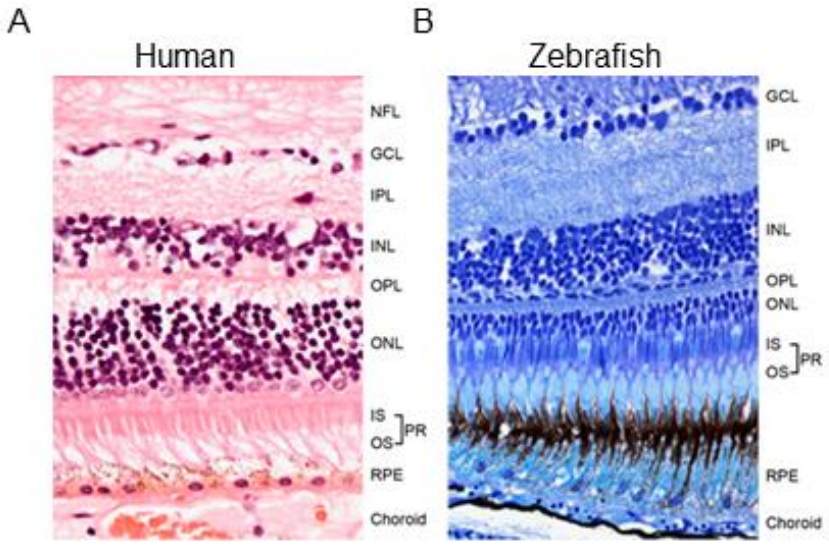

FIGURE 3 A CROSS-SECTION OF THE HUMAN AND ZEBRAFISH RETINA

(A) Human cross section of retina showing nerve fibre layer (NFL), ganglion cell layer (GCL), inner plexiform layer (IPL), inner nuclear layer (INL), outer plexiform layer (OPL), outer nuclear layer (ONL), inner and outer segment (IS and OS) of the photoreceptors (PR), retinal pigmented epithelium (RPE) and choroid. (B) A comparison to the zebrafish retina showing the similarities in structure and cellular arrangement. Image from Richardson et al., 2016.

1.5 Retinotectal Projections and Visual Function

In zebrafish, the retinotectal projection is formed by the RGCs connecting to the optic tectum. The RGCs extend axons along the inner surface of the retina, exit the eye via the choroid fissure and grow along the optic nerve. Here they continue to grow towards the optic chiasm where they cross at the midline, enter the optic tract, resort and continue to grow dorsally towards the contralateral optic tectum *(Figure 4A*; Erskine & Herreral, 2015; Malicki, Pooranachandran, Nikolaev, Fang, & Avanesov, 2016; Petros, Rebsam, & Mason, 2008).

The RGCs must be able to navigate through a variety of cellular environments and respond to internal and external cues to reach their final destination and form synapses with their target cells, therefore enabling proper formation of the sensory circuitry (Petros, Rebsam and Mason, 2008). It is thought that this guidance, from the start of their journey in the retina to their target destination of the optic tectum, is due to guidance molecules which either attract or repel the growth cones. These molecules can be diffusible or bound to their substrate (Petros, Rebsam and Mason, 2008).

In monocular vertebrates such as the zebrafish, the RGCs exit the eye and always cross the optic chiasm and therefore project to the contralateral optic tectum. However, in higher vertebrates that have binocular vision such as humans, only approximately 60% of RGCs will cross at this optic chiasm in the midline and project to the contralateral optic tectum. The remaining 40% of uncrossed axons will project to the ipsilateral optic tectum (Petros, Rebsam and Mason, 2008). In humans, defects in the formation of the optic chiasm are known to cause congenital ocular disorders such as nystagmus therefore affecting visual function including depth perception (Williams, Mason and Herrera, 2004; Petros, Rebsam and Mason, 2008).

In zebrafish, there are numerous examples of mutants that show defects in axonal pathfinding. One such mutant, *belladonna* has a mutation in the transcription factor *lhx2* that causes ipsilateral projections (*Figure 4*) and a reversed optokinetic response (OKR) (Karlstrom *et al.*, 1996; Seth *et al.*, 2006).

As visual function becomes apparent at 4dpf, zebrafish can be a model for the development of visual function. The optokinetic response is described as “an eye movement elicited by the whole field motion of the visual surround” (Mueller and Neuhauss, 2010). The response is spilt into two separate phases: the slow phase – the smooth pursuit of the stimulus in its perceived direction and once the eyes have reached their maximum deflection angle, the fast phase response of resetting in the opposite direction (saccade) (Beck *et al.*, 2004; Rinner, Rick and Neuhauss, 2005; Fadool and Dowling, 2008; Huang and Neuhauss, 2008; Mueller and Neuhauss, 2010).

This response can be quantified using an established set up where a visual stimulus such as rotating stripes on a drum, evokes an OKR which is tracked, allowing visual system defects to be detected, in addition to or despite any obvious anatomical phenotype (Fadool and Dowling, 2008; Mueller and Neuhauss, 2010).

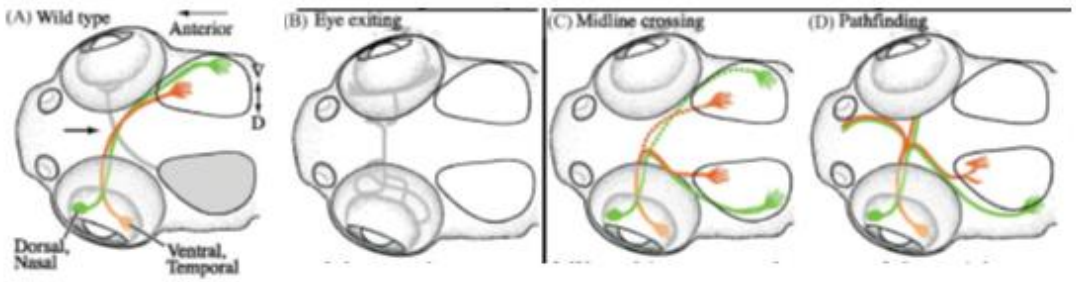

FIGURE 4 A SCHEMATIC OF RETINAL PROJECTIONS IN A WILD-TYPE AND MUTANT ZEBRAFISH

(A) The retinal projections can be seen exiting the eye, crossing at the optic chiasm (arrow) and entering the contralateral optic tectum in a wild-type. (B) A mutant with pathfinding defects on exiting the eye. (C) A mutant with defects in the midline crossing showing projections to both contralateral and ipsilateral optic tecta. (D) A mutant with pathfinding defects with projections observed in the telencephalon. Image from Culverwell and Karlstrom, 2002.

1.6 Vascularisation of the Optic Cup

The retinal vasculature provides oxygen and key nutrients to the highly metabolically active vertebrate eye (Bibliowicz, Rachel K. Tittle and Gross, 2011). In mammals, including humans the ocular vasculature is comprised of three different systems; hyaloid, retinal and choroidal vasculature. The hyaloid vasculature is the first to form with vessels entering the eye via the choroid fissure and forming a ring around the lens. The hyaloid vasculature will then connect to the superficial system that sits on top of the retina and will then regress so that a deep embedded choroidal vasculature system remains (Alvarez *et al.*, 2007; Kitambi *et al.*, 2009).

In zebrafish, the hyaloid vasculature will not regress but instead transitions into a mature retinal vasculature system that feeds the retina, whilst the choroidal vasculature becomes embedded deep within the retina and feeds the RPE as well as the photoreceptors with oxygen and nutrients (Alvarez *et al.*, 2007; Kitambi *et al.*, 2009; Weiss *et al.*, 2012; James *et al.*, 2016). The hyaloid artery enters the eye via the choroid fissure and will continue into the eye and branch into capillaries, the blood in this system will eventually drain through the hyaloid vein that exits via the choroid fissure (*Figure 5 A, B*; Kaufman et al., 2015). Hyaloid vessels branch off, move away from the lens and deflect onto the retina forming the superficial retinal vasculature (Kaufman *et al.*, 2015; James *et al.*, 2016; Richardson *et al.*, 2016). The superficial system is comprised of a ring-shaped vessel, the superficial annular vessel (SAV) and three branches; the nasal radial vessel (NRV), the dorsal radial vessel (DRV) and ventral radial vessel (VRV) (*Figure 5C;* Kaufman et al., 2015).

Numerous mutants in zebrafish with ocular phenotypes also display vasculature defects including; *lmo2*, *lama1* and *mab21l2*, showing that there is a link between the two phenotypes (Alvarez *et al.*, 2007).

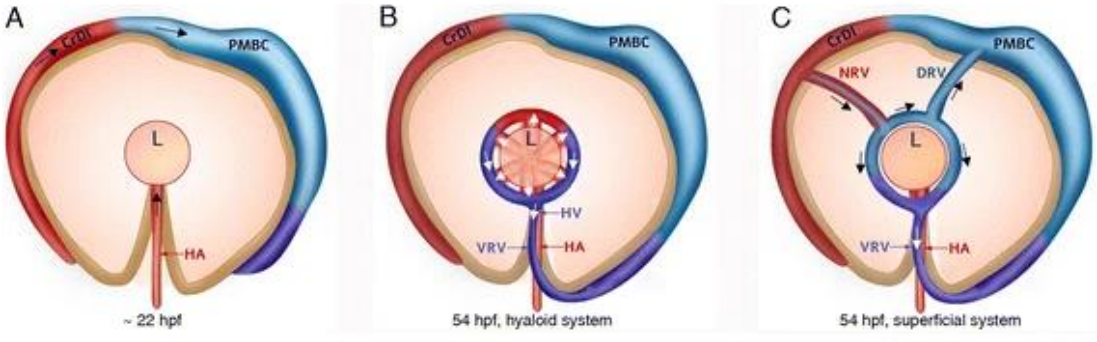

FIGURE 5 THE DEVELOPMENT OF THE HYALOID VASCULATURE IN THE DEVELOPING OPTIC CUP

(A) The hyaloid artery (HA) enters the eye via the choroid fissure. (B) Blood drains via the hyaloid vein (HV). (C) Hyaloid vessels branch off to form the superficial system. This consists of the nasal radial vessel (NRV), dorsal radial vessel (DRV) and the ventral radial vessel (VRV). Image from Kaufman et al., 2015.

1.7 The Choroid Fissure and Coloboma

1.7.1 Choroid Fissure Fusion

During the invagination of the optic vesicle, a transient opening forms in the ventral part of the eye, the choroid fissure (Bibliowicz, Rachel K. Tittle and Gross, 2011). The opening remains for the entry of the periocular mesenchymal (POM) cells to enter and help form the hyaloid vasculature and for the exit of the RGCs (*Figure 6 A, B).* Once this process has taken place, the apposing lips of the choroid fissure will come together, fuse and give rise to a continuous optic cup *(Figure 6C;* Bibliowicz et al., 2011a; Gestri et al., 2012; Richardson et al., 2019). Failure of fusion gives rise to a permanent opening known as coloboma (*Figure 6 D, E*), which may affect numerous structures of the eye including; retina, choroid, iris and optic nerve (Bibliowicz, Rachel K. Tittle and Gross, 2011; Bernstein *et al.*, 2018). In humans, coloboma is estimated to occur in 1 in 5,000 births and is one of the leading causes of congenital blindness with 10% of childhood blindness diseases due to this disorder (Bibliowicz, Rachel K. Tittle and Gross, 2011; Kathleen A Williamson and FitzPatrick, 2014; Bernstein *et al.*, 2018). Coloboma may occur bilaterally or monolaterally and its effect on visual function can range from complete

vision loss to asymptomatic (ALSomiry, Gregory-Evans and Gregory-Evans, 2019; Patel and Sowden, 2019).

Choroid fissure fusion is a unique epithelial fusion event since the two apposing surfaces are both basal, which differs to other epithelial fusion events such as neural tube closure in which the two fusing surfaces are both apical (Gestri, Link and Neuhauss, 2012; Bernstein *et al.*, 2018; Gestri *et al.*, 2018). Thus, the eye is surrounded by the basal membrane (BM), a component important in establishing and maintaining tissue borders, biomechanical strength and cell signalling and a critical component of the choroid fissure (Carrara *et al.*, 2019). The breakdown of the basal lamina is an essential event for choroid fissure fusion to take place (Hero, 1989; Gestri, Link and Neuhauss, 2012). This process allows the cells of both the nasal and temporal retina to repolarize and come together for fusion (Gestri *et al.*, 2018).

It is thought that POM cells and the formation of the hyaloid vasculature, help in the breakdown of the basal lamina allowing for fusion to take place (James *et al.*, 2016; Eckert *et al.*, 2017; Gestri *et al.*, 2018). As the POM cells enter the eye to help form the hyaloid vasculature, they can act as a scaffold between the apposing lips (James *et al.*, 2016; Eckert *et al.*, 2017). As such, the hyaloid vasculature is also a potential source of metalloproteinases which are suggested to be important in the dissolution of the lamina (Eckert *et al.*, 2017; Cao *et al.*, 2018; Gestri *et al.*, 2018). Moreover, mutants lacking early ocular vasculature and POM cells such as *cloche* and *lmx1b* have coloboma associated with defects in the breakdown of the basal lamina, indicating that these components are essential in facilitating the degradation of the basal lamina (Gestri, Link and Neuhauss, 2012; James *et al.*, 2016; Eckert *et al.*, 2017).

1.7.2 Mechanisms of Coloboma

Genetic as well as environmental factors have been implicated in ocular coloboma. Environmental causes included maternal deficiency in vitamin A and drug exposure, mainly alcohol and thalidomide (Gregory-Evans *et al.*, 2004; ALSomiry, Gregory-Evans and Gregory-Evans, 2019; Patel and Sowden, 2019). Genetically, only 20% of the causes of coloboma are known with causative mutations occurring in Pax2, Vax1, Vax2, BMPs, FGFs, SHH, Retinoic Acid and YAP1 (Kathleen A Williamson and FitzPatrick, 2014; Eckert *et al.*, 2017).

Coloboma can be split into two different main causes; the lack of apposition of the ventral and nasal retinas, and the lack of dissolution of the basal lamina in the choroid fissure. Lack of apposition of the temporal and nasal retinas are due to disruption in the early development of the optic cup and mutations in early patterning transcription factors such as *Pax6*, *Pax2* and *Shh* are all known to cause coloboma (Gregory-Evans *et al.*, 2004; Kathleen A. Williamson and FitzPatrick, 2014; ALSomiry, Gregory-Evans and Gregory-Evans, 2019; Patel and Sowden, 2019). Similarly, eye morphogenetic defects and coloboma have being associated with mutations in core POM cell transcription factors in different model systems (Eckert *et al.*, 2017; Gestri *et al.*, 2018; Patel and Sowden, 2019). Moreover, RPE fate controlled by the Wnt signalling pathway also has implications in choroid fissure fusion with mutations in *Fzd5* causing coloboma in humans (Liu *et al.*, 2016; Patel and Sowden, 2019).

Once the nasal and temporal lips are in contact, it is essential that the basal lamina lining each margin breaks down (Gestri, Link and Neuhauss, 2012; Bazin-Lopez *et al.*, 2015; Gestri *et al.*, 2018; Patel and Sowden, 2019). Mutations in laminins can lead to a persistent basement membrane and subsequently coloboma due to the inability of the nasal and temporal retinas to come into contact and fuse (Lee and Gross, 2007; Cao *et al.*, 2018). POM cells are thought to release enzymes (metalloproteinases) to help the dissolution of the basal lamina (Cao *et al.*, 2018; Patel and Sowden, 2019). Moreover, mutations in *talin1*, a gene that encodes a scaffold protein also shows persistence of the basal lamina and a coloboma phenotype demonstrating the importance of this aspect of choroid fissure fusion (James *et al.*, 2016; ALSomiry, Gregory-Evans and Gregory-Evans, 2019). Once the basal lamina breaks down, fusion is able to take place, resulting in a continuous neuroepithelium (Gestri *et al.*, 2018; Patel and Sowden, 2019).

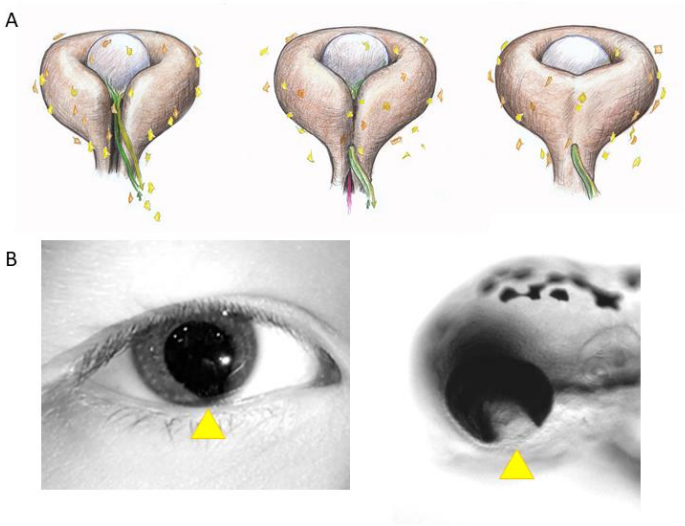

FIGURE 6 CHOROID FISSURE FUSION AND COLOBOMA

(A) POM cells (yellow stars) and hyaloid vasculature (green) entering the eye via the choroid fissure. (B) retinal axons (red) exiting the eye via the choroid fissure. (C) Choroid fissure fuses and forms a continuous optic cup. (Image from Gestri et al., 2012) (D) Example of coloboma in human patient highlighted by yellow arrow. (Image from Gregory-Evans, Williams, Halford, & Gregory-Evans, 2004). (E) Example of coloboma in zebrafish highlighted by yellow arrow.

1.8 The Role of the Extracellular Matrix in Optic Cup Morphogenesis

It is well known that the extracellular matrix (ECM) plays an important role in optic cup morphogenesis (*Figure 7A, B*; Kwan, 2014). Its role involves maintenance of mechanical stability, tissue development, formation of tissue barriers and promotion of cell dynamics such as migration, growth and adhesion (Zinkevich *et al.*, 2006; Varshney, Hunter and Brunken, 2015). The ECM also regulates polarity in numerous cell types such as neurons, epithelial cells and glial cells (Varshney, Hunter and Brunken, 2015). The ECM is primarily made up of four core components; laminins, nidogens, collagen VI and perlecan (Kwan, 2014; Varshney, Hunter and Brunken, 2015; Carrara *et al.*, 2019). Laminins have been well studied and are known to be essential in optic cup morphogenesis and choroid fissure fusion (Lee and Gross, 2007; Kwan, 2014; Carrara *et al.*, 2019). Moreover, it has recently been shown that in *nid1a/b* morphants, Nidogen is also essential in basement membrane remodelling during fusion and without this properly functioning protein there is disruption in the basement membrane breakdown and therefore a failure of the choroid fissure to fuse (Carrara *et al.*, 2019).

1.8.1 The Importance of Laminin in Optic Cup Morphogenesis

Laminins are core components of the ECM and are large glycoprotein heterotrimers (Zinkevich *et al.*, 2006; Varshney, Hunter and Brunken, 2015). Laminins consist of an alpha, beta and gamma chain. The heterotrimer Laminin1 comprised of: Laminin alpha1, beta1 and gamma1 being the most predominant found during the early stages of development (Varshney, Hunter and Brunken, 2015; Bryan, Chien and Kwan, 2016). Moreover, mutations in all three components of Laminin-111; *lama1* (*bashful; bal*), *lamb1* (*grumpy; gup*) and *lamc1* (*sleepy; slp*) present with brain and body defects. In addition, they also present ocular phenotypes such as retinal lamination issues, lens dysplasia and coloboma (Biehlmaier, Makhankov and Neuhauss, 2007; Pathania, Semina and Duncan, 2014).

1.8.2 Laminin is essential for apico-basal polarity

Apico-basal polarity is essential for the cell movements that drive optic vesicle morphogenesis (Hehr, Halabi and McFarlane, 2018). All eye field cells at this stage show apico-basal polarity markers and those situated on the surface of the bulging optic vesicles arrange their polarity to form a neuroepithelial sheet (Ivanovitch, Cavodeassi and Wilson, 2013). The evagination of the optic vesicles appears to be driven by cell intercalation of mesenchymal like progenitors into the neuroepithelial sheet (Ivanovitch, Cavodeassi and Wilson, 2013; Hehr, Halabi and McFarlane, 2018). This epithelialization requires the Laminin rich basal lamina. *laminin*γ*1* morphants showed that disruption of Laminin affects the polarity of the neuroepithelial cells which become disorganized with apical markers basally localised, rounded and only partial elongated (Ivanovitch, Cavodeassi and Wilson, 2013; Hehr, Halabi and McFarlane, 2018). However, despite these defects, the optic vesicles are still able to evaginate even though they are slightly delayed (Ivanovitch, Cavodeassi and Wilson, 2013). Moreover, in combination with reduced activity of *pard6*γ*b*, which encodes an apical protein, apico-basal polarity becomes compromised and the optic vesicles fail to evaginate (Ivanovitch, Cavodeassi and Wilson, 2013). Similarly in the absence of *laminin-alpha1*, apical proteins can be mis-localised, progenitors lose their apical attachments and subsequently optic cup morphogenesis is disrupted (Hehr, Halabi and McFarlane, 2018).

Moreover, a recent study into *traf4a*, a component of tight and adherens junctions reiterates the point that apico-basal polarity is essential in optic cup morphogenesis. Disruption of the *traf4a* gene causes apico-basal polarity defects in the neuroepithelium, cells lose their adherens junctions, they fail to elongate, their radial organisation becomes disrupted; hence evagination of the optic vesicles is asymmetric resulting in optic cups of different sizes (Hehr, Halabi and McFarlane, 2018). However, *traf4a* is not required for the subsequent event of choroid fissure fusion in optic cup morphogenesis (Hehr, Halabi and McFarlane, 2018).

It has been demonstrated that laminin is essential for the maintenance of epithelial polarity (Martin-Belmonte and Mostov, 2008; Bryan, Chien and

Kwan, 2016). In zebrafish, it is known that during optic vesicle evagination, zonula occludens (ZO-1) which is a component of tight junctions is located at the apical surface, that is opposite the laminin staining that surrounds the optic cup (*Figure 7C*; Bryan et al., 2016; Gestri et al., 2018; Ivanovitch, Cavodeassi, & Wilson, 2013). *lama1*^{uw1} mutant embryos displayed disruption to polarity with ectopic localization of aPKC and Par3, both apical makers, during optic cup morphogenesis. Therefore, laminin is essential in apico-basal polarity, with mutants displaying disruption to cell polarity throughout optic cup morphogenesis (Bryan, Chien and Kwan, 2016).

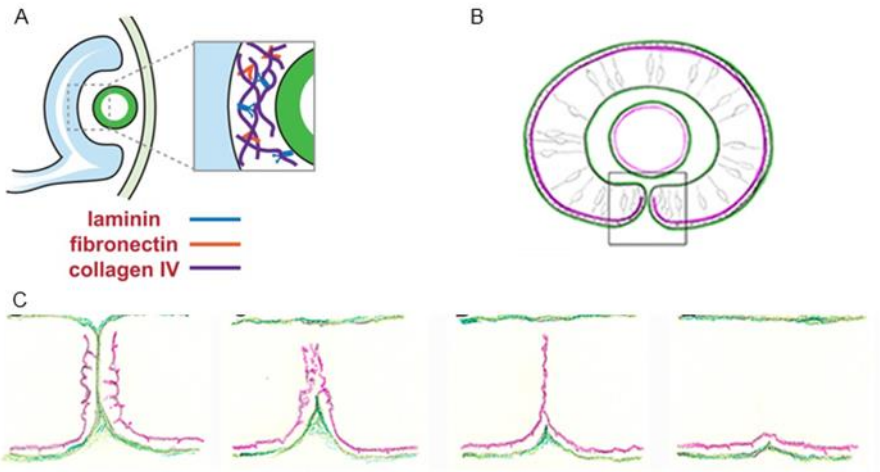

FIGURE 7 LAMININ AND ITS ROLE IN OPTIC CUP FORMATION
(A) A schematic of the structure of the basal laminin consisting of laminin in the optic cup (Kwan, 2014). (B) A drawing of the choroid fissure showing the basement membrane in green and Zo-1 in magenta. (C) Steps of basement membrane break down during choroid fissure fusion (Gestri et al., 2018).

1.9 A summary of Laminin associated studies in Zebrafish

Together, previous studies have determined that laminins are essential in the morphogenesis of the optic cup with various ocular phenotypes ranging from defects within the lens, cornea, retina, vasculature and retinal axon guidance being observed in mutants in these genes (Zinkevich *et al.*, 2006; Biehlmaier, Makhankov and Neuhauss, 2007; Lee and Gross, 2007; Martin-Belmonte and Mostov, 2008; Ivanovitch, Cavodeassi and Wilson, 2013; Pathania, Semina and Duncan, 2014; Bryan, Chien and Kwan, 2016).

bal^{a69} specifically has loss of the lens structure and ganglion cell layer disruption (Semina *et al.*, 2006; Zinkevich *et al.*, 2006; Pathania, Semina and Duncan, 2014). Axonal guidance defects were observed with routing errors of the axons towards the optic nerve head (Semina *et al.*, 2006). In addition, the photoreceptors are also affected with ectopic differentiation discovered within the inner retina (Semina *et al.*, 2006). Further, there was severe hyaloid vasculature dysmorphogenesis (Semina *et al.*, 2006).

In *bal*^{uw1} optic cup morphogenesis is disrupted with irregularities in optic cup formation and the lens structure (Bryan, Chien and Kwan, 2016). Initially, the RPE and NR fail to enwrap the lens, the lens structure itself appears flattened and ovoid in shape, further, the retina appears disorganized (Bryan, Chien and Kwan, 2016). Moreover, apico-basal polarity is disrupted in this allele, with ectopic localisation of apical markers and cells appearing to designate apical identity randomly and therefore resulting in multiple apical domains (Bryan, Chien and Kwan, 2016). In addition, there is a variation of routing errors of the RGCS, examples of; no crossing at the chiasm and only ipsilateral projections, axons projecting anteriorly towards the telencephalon and axons crossing at the midline but projecting ipsilaterally as well as contralaterally were all observed in mutants of this allele (Paulus and Halloran, 2006).

Moreover, *bal*^{tp82}, was found to have a wild-type like OKR but only at high intensities. The assumption in this study was that visual function could be disrupted at lower intensities due to lens dysmorphogenesis. In addition, Zpr-1 labelling shows that there was no disruption to photoreceptor morphology in

this allele, further indicating the variability between *lama1* alleles (Biehlmaier, Makhankov and Neuhauss, 2007).

Further, *bal*^{arl}*,* has a lens phenotype, by 5dpf the lens structure is absent with few cells and debris remaining where the lens should be (Vihtelic *et al.*, 2001). In addition, a study investigating the link between the lens structure and developing hyaloid vasculature in zebrafish found that between 3-6dpf in *bal*^{arl}, the intraocular vasculature is completely lost (Alvarez *et al.*, 2007).

Moreover, other laminins namely *lamb1* and *lamc1* show similar phenotypes including notochord, body axis and ocular defects (Biehlmaier, Makhankov and Neuhauss, 2007). Specifically, *lamb1* and *lamc1* both have a disrupted lens structure, retinal lamination issues with severe degeneration of the outer segment of the photoreceptors and synapses, rendering these animals blind (Biehlmaier, Makhankov and Neuhauss, 2007; Lee and Gross, 2007). In addition, *lamb1* and *lamc1* both present with coloboma, showing the importance of laminin in choroid fissure fusion (Lee and Gross, 2007; Patel and Sowden, 2019). However, *lama1* mutants described to date only show lens dysplasia and axonal misguidance (Zinkevich *et al.*, 2006; Pathania, Semina and Duncan, 2014; Bryan, Chien and Kwan, 2016).

1.10 Summary

To conclude, the genetic and morphogenetic bases of choroid fissure fusion are still largely unknown, with only 20% of genes associated with coloboma known so far. There are many different morphogenetic events that need to take place in a clear and coordinated manor to allow fusion to take place that by disrupting just one of these components can result in coloboma.

In this study, I will analyse two new alleles of *laminin alpha1* that display different severities of coloboma, which has not been previously described for mutations in this gene and compare these alleles to those already described.

I will also generate new tools to visualise choroid fissure fusion in particular focusing on the fate of the cells of the choroid fissure and how they enable fusion to take place.

2 Materials and Methods

2.1 Fish husbandry

Zebrafish embryos were obtained from natural spawning, raised at 28.5°C and staged according to hours or days post-fertilisation (hpf, dpf). To prevent pigmentation at 24hpf 0.003% 1-phenyl-2-thiourea (PTU) was added to the water. Previously established fish lines used in this study were as follows: *lama1*^{nl14} (also known as 308-6 coloboma), *lama1*^{nl15} (also known as Sauron) (both from Alex Nechiporuk), Tg(kdrl:eGFP^{s843}), Tg(atoh7:eGFP^{rw021}) and Tg(UAS:RFP;cry1:eGFP^{tp12}).

2.2 Histology

2.2.1 Immunolabelling of Cryosections

Embryos were fixed in 4% PFA (w/v) overnight at 4°C before being sequentially incubated in 15% and 30% sucrose in phosphate-buffered saline (PBS) for an hour and then embedded in OCT, set on dry ice and sectioned at 20µM using a Leica CM1510S cryostat. The following steps were carried out at room temperature (RT). The sections were left to dry on the slide for approximately 30 minutes before being washed in 1X PBS (without detergent) 2x 10 minutes and blocked with 10% Heat Inactivated Natural Goat Serum (Sigma, Cat#G9023) in PBS for at least one hour. They were incubated overnight with the primary antibody, mouse monoclonal anti-Zpr1 (Abcam, #ab174435) diluted 1:200 in block solution.

On the second day, the primary antibody was removed by washing the slides for 3x 10 minutes with PBS. The slides then went through a secondary antibody incubation for one hour at RT, using Alexa 488 mouse conjugated secondary antibody (dilution 1:200, Invitrogen, #A11029) and DAPI, a nuclear stain (1:500, Abcam, #ab228549) in block solution. The secondary antibody was removed, and the slides were washed a further 3x 10 minutes in PBS. On the final wash the PBS was removed as much as possible from the slides to ensure the sections were dry. The slides were then mounted with Citifluor glycerol/PBS (Science Services, #E17970-100) and covered with a VWR

Thickness No.1 coverslip (approximately 130-160 μm). To ensure the coverslip did not move once the slide had been set with glycerol, clear nail varnish was used to seal the coverslip to the slide.

Imaging was acquired on the Lecia SP8 confocal, see Imaging Acquisition.

2.2.2 Whole-mount Immunohistochemistry

Embryos were fixed with 4% PFA (w/v) at specific timepoints e.g. 72hpf, at RT for one hour and further preserved in 100% methanol at -20°C until required. To rehydrate the embryos from methanol they were serially washed with 75/25, 50/50, 25/75 methanol/PBSTr until they hit 100% PBSTr. They were further washed in 100% PBSTr for 4x 5-minute washes. To permeabilize the embryos, we used proteinase K (0.02 mg/mL) at different concentrations depending on the stage from 1X to 4X for 30 minutes. They were post fixed in 4% PFA (w/v) and further washed in PBSTr for 4x 10 minutes. They were incubated in 10% Heat Inactivated Natural Goat Serum (Sigma, Cat#G9023) in PBSTr and 1% Dimethylsulfoxide (Sigma, Cat#276855) block solution for at least one hour at RT on the shaker. Primary antibody incubation was carried out overnight at 4°C in block solution using the following antibodies: chicken polyclonal anti-GFP (dilution 1:500, Abcam, #ab13970) and rabbit polyclonal anti-Laminin (dilution 1:100, Sigma, #L9393).On the second day, the antibody was removed and the samples were washed all day with PBSTr (at least 6x 30 minutes) to remove any residual primary antibody. Secondary antibody incubation was carried out over night at 4°C using, Alexa 488 chicken (dilution 1:200, Invitrogen, #A11029), Alexa 633 rabbit (dilution 1:200, Invitrogen, #A21071) and DAPI (1:2,000**,** Abcam, #ab228549) in block solution. On the third day, the secondary antibody was removed, and the samples washed at least 6x 30 minutes with PBSTr, prepared for mounting and imaging (see Imaging Acquisition).

2.2.3 Retinal Axon Tracing with DiI and DiD Labelling

Tracing of the retinal projections from the eye to the optic tecta was carried out by labelling with membrane-bound lipophilic dyes DiI (DiIC18(3), Molecular Probes, Cat# D3911) and DiD (DiIC18(5), Molecular Probes, Cat#D D7757) in 5 dpf larvae that had been post fixed in 4% PFA (w/v) after performing OKR. After being fixed overnight at 4°C the larvae were transferred to PBS. The dyes were prepared by dissolving equal weight of crystals to volume of chloroform and the solution spread over a slide to acquire small crystals or the dye was injected as an aqueous solution. Two methods were used to try to obtain the best results; the dyes were either placed into a microinjection needle and injected behind the lens or using tungsten needles that were sharpened by electrolysis in concentrated NaCl, dotted onto the slide with crystals and then applied behind the lens of the eye. The embryos were left at 4°C overnight to allow the dye to travel through the retinal axons to their destination – the optic tecta. The embryos were prepared for imaging - see image acquisition.

2.2.4 Whole mount in situ hybridisation

For *in situ* hybridisation probes, linear DNA templates were produced from a cDNA library from WT 48hpf embryos using RT-PCR (TABLE 1)and tagged with T3. Antisense RNA probes were synthesised using T3 polymerase (Promega, Cat#P2083) and digoxigenin labelled nucleotides (Roche Cat# 11277073910) and incubated at 37°C for two hours. The probes were then purified using a QIAGEN RNeasy kit (Cat# 74106) and eluted in 30µl nuclease free water and tested on a 1.5% Trisacetate-EDTA (TAE) buffer (40 mM Tris, 20 mM acetic acid, 1 mM EDTA).

Embryos were fixed with 4% PFA (w/v) at specific timepoints e.g. 72hpf, at 4°C overnight. They were further preserved in 100% methanol at -20°C until required. To rehydrate the embryos from methanol they were serially washed with 75/25, 50/50, 25/75 methanol/PBSTween until they hit 100% PBSTw. They were further washed in 100% PBSTw for 4x 5-minute washes. To permeabilize the embryos, we used proteinase K (0.02 mg/mL) at different concentrations depending on the stage from 1X to 4X for 30 minutes. They were post fixed in 4% PFA (w/v) and further washed in PBSTw for 4x 10 minutes. They were incubated in hyb+ containing 50% formamide for at least two hours at 68°C before being incubated overnight with the previously made probes at a dilution of 2ng/µl at 68°C.

On the second day the probe was recovered from the embryos and they were washed at 68°C through a serially graded hybridisation solution and 2X Saline Sodium Citrate (SSC) at (100, 75, 50 and 25%) for 15 minutes per wash. They were then washed 2x 30 minutes in 2X SSC and a further 2x 30 minutes in 0.2X SSC. They were further washed through a graded series of 0.2x SSC and PBSTw (100, 75, 50 and 25%) for 10 minutes each and then a further 2x 10 minutes in PBSTw at room temperature and then incubated in maleic acid block (150 mM maleic acid, 100 mM NaCl, 2% sheep serum, 2 mg/ml BSA) for at least two hours at room temperature. Finally, they were incubated overnight at 4°C with Anti-Dig POD Fab Fragments (dilution, 1:6,000; Roche, cat#16646820) in MaBl.

On the third day the antibody was removed, and embryos were washed for 4x 30 minutes with PBSTw to remove as much excess antibody as possible. They were washed for 3x 5 minutes with AP buffer (5ml 1M Tris pH 9.5, 2.5ml 1M MgCl2, 1ml 5M NaCl, 500µl 10X Tween and made up to 50ml with MiliQ Water). The embryos were then placed in a staining solution consisting of 1µl/mL Nitro Blue Tetrazolium (NBT) and 3.5µl/mL 5-Bromo-4-chloro-3-indolyl phosphate (BCIP) (Roche, Cat# N6876 and 11383221001) in AP buffer. The time of this stage is dependent on each probe and how quick the staining comes through, generally between 1-5 hours. Once the embryos have been incubated sufficiently to see expression profiles for each probe, the stain was removed with PBSTw and the embryos were further fixed in 4% PFA (w/v).

2.2.5 Plastic Sectioning

Embryos were fixed overnight at 4°C in 4% PFA (w/v). The next day they were washed in 1X PBS 3x 5 minutes. They were further washed 3x 10 minutes in MiliQ water. For dehydration into ethanol they were serially washed in 30% ethanol/70% water, 50%/50%, 70%/30%, 95%/5% and 100% ethanol each for two minutes. The embryos were then processed using the JB-4 embedding kit (Sigma, #EM0100). An infiltration solution was made up by mixing 25 ml of JB-4 Solution A (monomer, Sigma cat#J4954) and 0.36g benzoyl peroxide (catalyst, Sigma cat#J0455). The embryos were then placed in 1:1 infiltration solution and 100% ethanol for one hour at room temperature in the dark. After this the samples were further incubated in 100% infiltration solution overnight on a shaker at 4°C.

The following day the embryos were embedded in a rubber embedding mould and set in 175µl of resin (40µl JB-4 Solution B (polymer, Sigma cat# J0330) to 960µl of infiltration solution). The mould was placed in a box with liquid nitrogen to remove any oxygen allowing the resin to set. This was done for approximately 2 hours to overnight depending on the rate the resin was setting.

The next day the samples were mounted using a mix of 1g of dibenzoyl peroxide (Sigma, #517909) and 500µl of methyl methacrylate (Sigma, #M55909) to set the resin sample onto a mounting block and further placed on the Leica JungRM2055 microtome and orientated for cutting. Sections were taken at 14µM and placed in a droplet of water on a slide, the slides were then dried on a heat block set at 37°C.

Once completely dried and set, the sections were stained with a toluidine blue stain; 1% toluidine blue (Sigma, #M55909) and 1% borax (Sigma, #B9876) made up in MiliQ water, for 30 seconds and rinsed with distilled water until all the excess stain was removed. Sections were further left to dry and mounted with VWR Thickness No.1 coverslips (approximately 130-160µm) using DPX glue (Merck, #HX55746679). Imaging was performed as described in imaging acquisition.

.

2.3 Image Acquisition and Analysis

2.3.1 Confocal Microscopy

Confocal imaging was carried out using Leica TCS SP8 system with a 25x/0.95 NA PL FLUOROTAR water-dipping objective (Leica) for live-imaging or 25x/0.95 NA PL IRAPO water-immersion objective with coverslip correction (Leica) for samples that were fixed. During live imaging, embryos were kept at 28.5°C for normal development. Whole mount immunohistochemistry samples were mounted in 1.5% low melting point agarose (Sigma, Cat# 16520050), using glass rings fitted on a slide by silicone grease and VWR Thickness No.1 coverslips (approximately 130-160µm). Immunolabelled cryosections were imaged with a 63x/1.3 NA HCX PL APO oil-immersion objective (Leica). Imaging was performed by scanning at 600 Hz, with 1024x1024 pixel resolution, line averaging of 3-4 and z-step size of 1µm. Sequential scanning was used for samples labelled with DAPI to avoid bleed through in other channels.

2-photon imaging was carried out on the Brooker Instruments 2-photon microscope with a 20X 1.0na water-dipping objective (Brooker Instruments).

Imaging was performed by scanning at 600Hz, with 1024x1024 pixel resolution, line averaging 3-4 and z-step size of 1µm.

Maximum projections for z-stacks were created using Fiji (ImageJ) software. Images and figures were assembled using Microsoft PowerPoint.

Imaging of whole mount *in situ* samples and plastic sections were performed on the Nikon Eclipse Ni with Fluor 40X/0.80W or 20X/0.40A objectives (Nikon). Images were taken using LAZ software. Whole mount embryos were processed in serial glycerol dilutions 20/40/60/80% before being mounted on a glass slide and covered with a cover slip. Images were taken using LAZ software.

2.3.2 Electron Microscopy

Half strength of the original fixative formulation (Karnovsky, M.J. 1965) was used: 2.5% glutaraldehyde, 2% formaldehyde in 0.1M cacodylate buffer and 25mg $CaCl_2$/100ml for less shrinkage of tissue. Samples were then processed by washing 2x 10 minutes in 0.1M Sodium Cocodylate buffer (CaCO). This wash buffer was then removed and a mix of 1:1 2%OSO_4 and 2.0M CaCO (creating a working concentration of 1%/0.1M) was added to the samples and incubated at 4°C in the dark for approximately 90 minutes. This mix was removed, and the samples washed for 10 minutes in 0.1M Sodium Cocodylate. The samples were washed in distilled water 2x 10 minutes and then incubated in Enbloc stain with 2% uranyl acetate in dH20 for 40 min. This mix was removed, and samples were washed in distilled water 2x 10 minutes. Samples were then gradually dried out in serial dilutions of ethanol: 25%, 50%, 70%, 90% for 10 minutes per wash and then 100% ethanol 4x 10 minutes. The ethanol was removed from the sample and soaked in Propylene Oxide 3x 10 minutes, taking care not to let the sample dry out in between.

Samples were embedded in resin by serial washes in differing ratio mixes. A 1:2 ratio mix of Propylene Oxide and resin (6g Agar 100 Resin, 4g DDSA and

2.5g MNA), a 2:1 mixture and 1:2 mixture and incubated for 30 minutes per mix. Finally, this mix was replaced with 100% resin and left overnight. The following morning the old resin was replaced for fresh resin.

Semi serial sections were cut on Reichert ultra-cut S microtome and collected on Formvar slot copper grids and stained with lead citrate. The samples were then viewed with a Joel 1010 transition electron microscope and the images recorded using a Gatan Orius CCD camera.

2.4 Molecular Biology

2.4.1 Mapping

Genomic DNA extracted from *lama1*^{nl15} 3dpf embryos was sequenced and processed by the Institute of Neurology HiSeq3000 Sequencing Systems with a 1x 200 base pair reads output.

Extracted RNA from *lama1*^{nl14} was sequenced by the Institute of Child Health Genomics Microarray and High Throughput Sequencing (HiSeq).

All samples for WGS and RNA seq were taken from 3dpf whole embryos. Mutants were selected based on the presence of a coloboma phenotype only.

For data analysis, we used a modification of the Cloudmap tool (http://usegalaxy.org/cloudmap; Minevich *et al.*, 2012) that uses local regression to highlight genomic regions which are homozygous in the mutant sample and heterozygous in the sibling sample. After a candidate region was identified, a list of candidate SNPs was produced by filtering for SNPs which appeared at greater than 90% frequency in the mutant sample and less than 50% in the sibling sample. We then used Ensembl's variant effect predictor to identify which of these SNPs were potentially deleterious.

2.4.2 Sanger Sequencing

To confirm *lama1*^{nl14} SNP, genomic DNA from embryos with and without a clear phenotype was extracted via HotSHOT genomic DNA extraction. RT-PCR was performed with *lama1* primers (TABLE 1) made around the point of mutation. Products were cleaned up using EXOSAP-IT (Applied Biosystems, #78201-1mL) and sent for Sanger sequencing at Source Biosciences. Sequencing results were analysed via Benchling.

2.4.3 Genomic DNA Extraction – HotSHOT technique

For genotyping of embryos and adults we used the KASP technique. First, DNA was extracted from tail clippings or embryos by a HotSHOT DNA extraction technique (Meeker et al., 2007). The sample is placed in alkaline

lysis solution (25 mM KOH, 0.2 mM EDTA, pH 12) for 30 minutes at 95°C. Once the incubation was complete, the reaction was neutralized with an equal volume of neutralizing solution (40 mM Tris-HCl, pH 5).

2.4.4 Genomic DNA Extraction – QIAGEN technique

Genomic DNA was extracted from 93 sibling and 93 mutant *lama1*^{nl15} whole embryos at 3dpf using the QIAGEN Puregene Core Kit A (QIAGEN, #158667). Embryos frozen liquid nitrogen were homogenised with a mortar and pestle. To each sample, 900µl of cell lysis solution was added and incubated at 65°C for 1 hour. A volume of 4.5µl of 20mg/ml of Proteinase K per sample was added and further incubated at 55°C overnight. The following day, 4.5µl of RNase A solution at concentration of 4mg/ml was added and the samples incubated at 37°C for 2 hours. The samples were quickly cooled on ice for 1 minute. Once cool, 300µl of protein precipitation solution was added and vortexed for 20 seconds. The samples were centrifuged at room temperature at 13,000rpm for 3 minutes. The supernatant was transferred to a clean Eppendorf with 900µl of isopropanol. This mix was centrifuged for 1 minute and the supernatant discarded. To wash the DNA pellet 300µl of 70% ethanol was added and centrifuged for 1 minute. The ethanol was carefully removed, and the pellet left to air dry for 10 minutes. Finally, 100µl of DNA hydration solution was added to the pellet and incubated at 65°C for 1 hour to dissolve the DNA.

2.4.5 RNA Extraction

For each condition embryos were collected and homogenized in 500µl of TRIZOL solution (Invitrogen, #15596018). Once the tissue had appeared to be fully homogenized, it was left for 5 minutes at room temperature. After this, 100µl of chloroform was added to each sample, hand shaken for 15 seconds, and left for 3 minutes at room temperature. The tubes were then centrifuged at 4°C at 12,000g for 15 minutes (same temperature and speed throughout). Approximately 200µl of the supernatant was transferred to a clean eppendorf where 166.5µl of isopropanol was added and mixed. This was then left for a further 10 minutes at room temperature. The samples were then centrifuged

for 10 minutes and the pellet was then washed 3x with ice-cold 75% ethanol and spun for 5 minutes each time. After the third wash, the pellet was left to air dry and re-suspended in 30µl RNase free water.

2.4.6 cDNA Synthesis

cDNA was synthesised from the extracted RNA using the LunaScript™ RT SuperMix Kit (NEB, #E3010). A mix of 4µl LunaScript™ RT SuperMix (5X) with up to 1µg of RNA sample was made up to 20µl total with RNAse free water. This mix was then placed on a thermocycler and run with the conditions; primer annealing at 25°C for 2 minutes, cDNA synthesis at 55°C for 10 minutes and heat inactivation at 95°C for 1 minute.

2.4.7 Kasp

Kasp was used to genotype *lama1*^{nl14} (T-C) and *lama1*^{nl15} (T-A) lines. A master mix of 4µl 2Xkasp buffer, 0.11µl primers (TABLE 2) and 3µl of Nuclease free water was made. This master mix was distributed into the wells of a white 96 well plate. 1µl of DNA was then added to each individual well. The plate was run on the PCR thermocycler using the following programme; 94°C for 15 minutes, 1 cycle; 94°C for 20 seconds, 1 cycles; touchdown over 65-57°C for 60 seconds, 10 cycles dropping 0.8°C per cycle; 94°C for 20 seconds, 57°C for 60 seconds, 26 cycles. The analysis of the allelic distribution was performed using the Bio-Rad CFX Manager 3.1 software.

2.4.8 RT-PCR

All RT-PCR experiments used a PCR master mix of 1.25µl 10X PCR buffer, 0.375µl 50mM $MgCl_2$, 0.5µl 10µM forward and reverse primer mix (TABLE 1), 0.25µl dNTP mix, 1µl of template DNA (can vary according to concentration of template DNA), 0.125µl *Taq* DNA polymerase and made up to 12.5µl with nuclease free water (*Taq* DNA Polymerase, recombinant, Invitrogen, #10342020). The RT-PCR was performed on a thermocycler (Eppendorf/vapo prot) at standard conditions: 95°C for 5 minutes, 95°C for 30 seconds, 55°C-

65°C (depending on primer) for 30 seconds, 72°C for 30 seconds, steps 2 to 4 repeated for 35 cycles, 72°C for 5 minutes and hold at 4°C.

For sequencing, a high fidelity *Taq* was used. In this instance Q5® High-Fidelity DNA Polymerase (NEB, #M0491) was used in a combination of; 2.5µl Q5 reaction buffer, 0.25µl 10mM dNTPS (Promega, #U1330), 1.25µl 10µM forward and reverse primer mix, 0.125µl Q5 high-fidelity DNA polymerase, 1µl template DNA (can vary) and made up to 12.5µl with nuclease free water. The samples were placed on a thermocycler at conditions suggested by the manufacturer as follows: 98°C for 30 seconds, 98°C for 10 seconds, 55-65°C (depending on primer) for 30 seconds, 72°C for 20 seconds, repeat steps 2 to 4 for 35 cycles, 72°C for 2 minutes and hold at 4°C.

2.4.9 Quantitative PCR

Primers were designed for *lama1* in the exons which were flanked by the biggest introns (TABLE 3). TRIZOL RNA extraction was used to acquire wildtype RNA from wild-type embryos for primer testing and *lama1*^{nl15} RNA from embryos with (mutants) and without (siblings) a clear phenotype for the final experiment. cDNA was made from these samples and used for the qPCR reaction. The cDNA was diluted 1:5, 1:25, 1:125 and 1:625 and for each primer there were three replicates. A master mix using the GoTaq® qPCR Master Mix (Promega, #A6002) was made with 5µl GoTaq and 2.5µl of nuclease free water. For the qPCR reaction 7.5µl of the master mix was added to each well of a 96 white PCR plate. To each individual well, 0.5µl of 10µm mix of forward and reverse primer was added and then again to each well 2µl of cDNA was added. The plate was run on Bio-Rad CFX96 Real Time System C1000 Thermal Cycler machine at standard conditions: 50°C for 10 minutes, 95°C for 5 minutes, 95°C for 10 seconds, 60°C for 30 seconds, the latter two steps were repeated for 39 cycles and the run ended. From the data, the efficiency of each primer was calculated by plotting log concentrations over the control value. Efficiency = 10^(-1/slope). From calculating the efficiency of the test primers, the most efficient primer set were used for the run, comparing wild-type siblings to mutants. The average of the triplicate samples was

calculated for both siblings and mutants. The data was further processed by normalising the data to the average from the wild-type and then comparing the mutant to this wild-type value. Analysis and statistics were performed using Microsoft Excel and GraphPad Prism 6 software.

2.4.10 Capped mRNA in vitro Synthesis for Microinjection

Pard3:GFP plasmid was linearised overnight at 37°C with Not1 enzyme (Promega) and transcribed with the MEGAscript SP6 kit (Ambion, #1330) according to manufacturer's instructions and incubated at 37°C overnight.

CRISPR/cas9 guides against *netrin1a* (TABLE 4) were found using the ChopChop software. Cas9 RNA was generated using the T3 mMessage machine kit (Ambion, #1348) and guide RNA was generated with the MEGAscript T7 kit (Ambion, #1334) according to manufacturer's instructions and incubated at 37°C overnight.

Residual DNA was removed using Turbo DNase and further incubated at 37°C for 15 minutes. RNA was purified by standard ammonium acetate precipitation. First by adding a mix of 10µl 5M ammonium acetate and 60µl 100% ethanol and incubating at -80°C for 20 minutes or -20°C overnight. The sample was spun down at 4°C for 15 minutes and the pellet was washed with ice cold 70% ethanol, centrifuged for a further 5 minutes at 4°C and the pellet left to air dry. The RNA was resuspended in 30µl RNase free water. Samples were checked by running on a 1.5% TAE gel.

2.4.11 Plasmid DNA Synthesis

A scraping from glycerol stocks of Gal4FF was inoculated onto LB agar plates with kanamycin and grown overnight at 37°C. The following day positive colonies were collected and incubated in LB broth with kanamycin on a 37°C shaker overnight. The samples were then miniprepped using PureLink™ HiPure Plasmid Miniprep Kit (Invitrogen, # K210003) according to manufacturer's instructions. The remaining DNA pellet was left to air dry for 10 minutes and was resuspended in 50µl nuclease free water.

2.4.12 CRISPR/Cas9 Microinjections

Microinjections were performed on embryos at one cell stage with concentrations of 75pg sgRNAs, 150pg cas9 and 100pg of plasmid DNA.

Testing of guides were performed by extracting genomic DNA from embryos at 24hpf and running a high-resolution melt analysis (HRMA). A master mix was set up with 5µl high resolution master mix (Bio-Rad, #172-5112), 1µl 10µM forward and reverse primer mix (TABLE 4) and 3µl MiliQ Water. For the HRMA reaction, 9µl of master mix was distributed in a white 96 well plate and to each well 1µl of genomic DNA was added. The plate was run on the Bio-Rad CFX96 Real Time System C1000 Touch Thermal Cycler at standard conditions of: 95°C for 2 minutes, 95°C for 10 seconds, 60°C for 30 seconds, 72°C for 30 seconds and steps two to four repeated for 40 cycles; 95°C for 30 seconds, 60°C for 1 minute, 0.2°C increments from 65°C to 95°C at 10 seconds per step. Analysis was performed using the Bio-Rad Precision Melt Analysis software.

2.5 Optokinetic Response

This investigation was performed by a custom-built optokinetic response rig which tracks the horizontal eye movement in response to whole-field motion. *lama1*^{nl14} larvae with coloboma and siblings were embedded at 5dpf in 2% low melting agarose and once set, the agarose was cut from around the eyes, freeing them to move as normal. The larvae were placed on a stage with a surrounding drum 25 mm from the center of the fish's head, where square box gratings were presented at differing sizes, contrasts and speeds by a MicroVision SHOWWX+ projector. Eye movements were tracked under infrared illumination (720nm) at 60 Hz using a Flea3 USB machine vision camera and custom-written LabView software. The gain of each eye (degrees/second) was processed via custom-written MATLAB code.

RT-PCR Primer	Forward	Reverse
lama1nl14	GTTGTTGCATGCATCCGTAG	ATCATCATTAAAGCAGCAAACTCTCCTCG
pth2	TTCACACTGGCACCTGACAA	**AATTAACCCTCACTAAAGGG**TCTGCATATAGGAGTTGAGCCA
clu	TCATGTCGTCAACATCAGCCA	**AATTAACCCTCACTAAAGGG**GCCCACCAAACATACTGGGA
eif1b	CGTTTCGGGTGACGTCATGT	**AATTAACCCTCACTAAAGGG**CCTTGTCGTCTGTCCATGCT
sepw2a	GCCACCCAAGATGTAAGGGA	**AATTAACCCTCACTAAAGGG**ACAACCAGCCACAGATGAACA
kidins220a	CCGGCCTTACTTCCCTCATC	**AATTAACCCTCACTAAAGGG**TTTGCCAAAGGGTTTGCGTC
mmda2a	ATTCCCAGTATCTTGGGCGG	**AATTAACCCTCACTAAAGGG**TCAGGCTTCAGACCGTACAAC
uqcrh	TGATAAACAAACACTGACCGCA	**AATTAACCCTCACTAAAGGG**AGACTGTGTCACCATCTATGAGG

TABLE 1 TABLE OF RT-PCR PRIMERS

Kasp	x	y	c
lama1nl14	GAAGGTGACCAAGTTCATGCTGTTCGTCCTGCAGGTGTT	GAAGGTCGGAGTCAACGGATTGTTCGTCCTGCAGGTGTC	CGAGGAGAGTTTGCTGCTTTAATGATGAT
lama1nl15	GAAGGTGACCAAGTTCATGCTGTGGAGCACTGTGAGTGT	GAAGGTCGGAGTCAACGGATTGTGGAGCACTGTGAGTGA	GTTACCTCACAGGAAGTGCCTGAATA

TABLE 2 TABLE OF KASP PRIMERS

qPCR	Forward	Reverse	Efficiency
lama1 exon 3+4	ATCAAGAACGGCCGTCAGTT	ATCCAGTTTCCAGGTCGAGG	2.82
lama1 exon 6+7*	CATCTCAGTGGGCGGGATG	TGGTATCCAGGACAACACTCA	1.07
lama1 exon 13+14	CACTGCGCTCACACTTCAG	GCCGCTGTGTGAGTCTATGA	1.11

TABLE 3 TABLE OF QPCR PRIMERS

CRISPR	Forward	Reverse	Guide
netrin1a	GAAAGACACAGA AACTGCCACA	GGATACTGGAGG TAATTGTCCG	TCGGTCAGGTAAGCTGGT GTTTTTAGAGCTAGA
Gal4FF-midCDS	TCCCTTGTTTGAG GACTCCTC		
Gal4FF-STP	TCAGTTTCCTGG CAGCATATC		

TABLE 4 TABLE OF CRISPR PRIMERS AND GUIDES

3 Results

3.1 *nl14* and *nl15* present with ocular coloboma

To identify genes contributing to eye morphogenesis, zebrafish families carrying ENU-induced mutations were screened for the presence of coloboma, a failure in the closure of the choroid fissure of the eye. Two recessive mutations with different severities of ocular coloboma were recovered, *nl15* mutants display a more severe coloboma phenotype associated with lens extrusion and anterior-posterior (AP) body axis defects with tail curled upward (*Figure 8B, B'*). In contrast, *nl14* homozygotes have a mild coloboma sometimes associated with the presence of ectopic retina extending from the eye to the diencephalon as highlighted by the yellow arrow in *Figure 8D'*. This phenotype is not fully penetrant and variable between clutches, coloboma is present in only 30-40% of the mutants; the penetrance increases to 55-85% when fish are raised at higher temperature (32°C).

Histological sections were performed to further analyse the ocular phenotypes. At 3dpf, both lines have fully formed and differentiated retinal layers as in control eyes (*Figure 8E, F, G*). Sections showed the lack of a fully formed lens in *nl15* mutants (*Figure 8F*) and the presence of neural retina extruding to the diencephalon in *nl14* (*Figure 8G*).

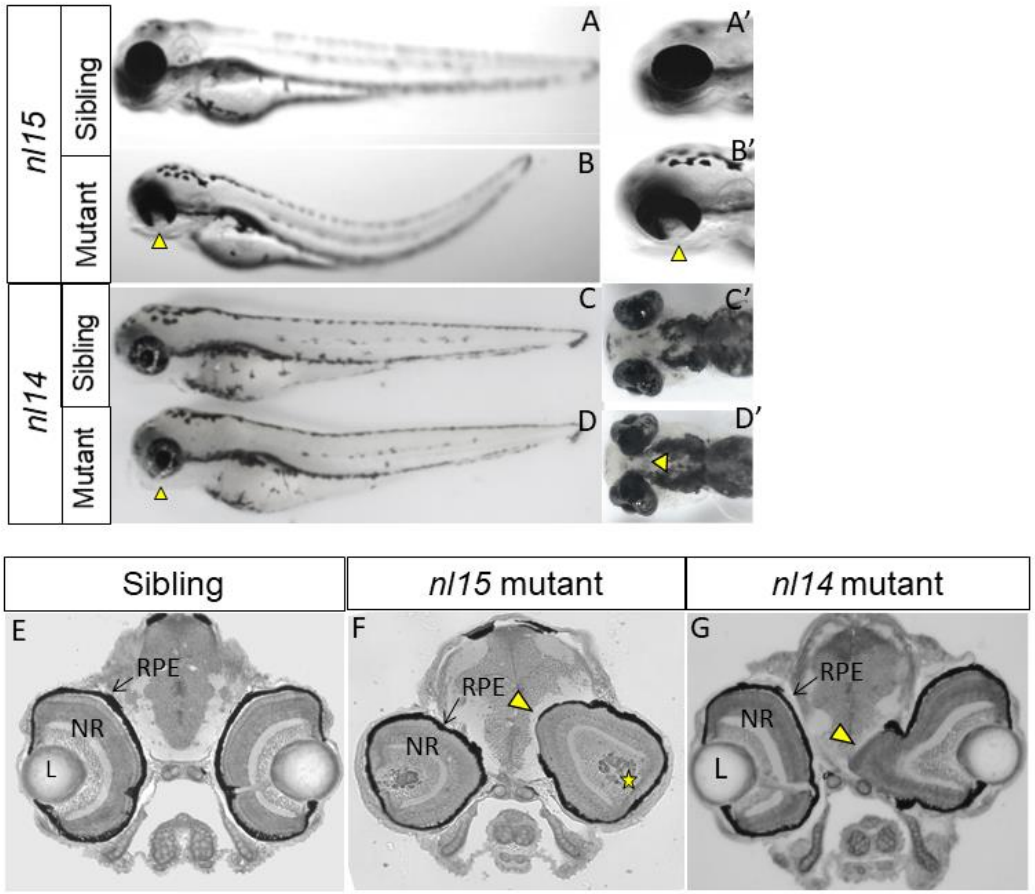

FIGURE 8 COLOBOMA PHENOTYPE IN *NL14* AND *NL15*

(A, C) 5dpf siblings and (B, D) mutants. (A') *nl15* sibling and (B') mutant at higher magnification focusing on the eye, arrows show the position of the coloboma. Dorsal view of sibling (C') and *nl14* mutant (D') showing the extrusion of the ventral retina into the diencephalon highlighted by the arrow. (E-G) Plastic sections of sibling, *nl15* and *nl14* retinas where L is the lens, NR the neural retina and RPE is the retinal pigmented epithelium. The yellow arrow indicates the ectopic extrusion of the retina in both F and G. In addition, the star in F highlights the lack of a lens structure in the eye of the *nl15* mutants.

3.2 Both *nl14* and *nl15* are mutations in the *laminin alpha1* gene

ENU mutagenesis causes single nucleotide polymorphisms (SNPs) (de Bruijn, Cuppen and Feitsma, 2009). To identify the causative mutations in both the coloboma lines we used two different approaches: whole genome sequencing (WGS) and RNA sequencing.

Whole genome sequencing of DNA from 3dpf whole embryos (93 sibling and 93 embryos with a coloboma in the *nl15* allele), localised the mutation on chromosome 24 between 35 and 45 Mb (*Figure 9B*). Only one stop codon was found in the interval; a non-sense point mutation in *laminin alpha1* (*lama1*), a T-to-A, located in position 41827109mb. This mutation is predicted to generate a truncated protein of 713aa, instead of 3075aa, lacking the LamB, EGFlike and LamG domains *(Figure 9D).* Previous studies have shown ocular phenotypes such as lens extrusion, in other *lama1* alleles, confirming it is the likely candidate gene for harbouring the mutation (Zinkevich *et al.*, 2006).

Quantitative PCR of *lama1* sequence in siblings versus mutants was performed to investigate whether there was nonsense mediated decay (NSMD) in *lama1*^{nl15} embryos. The NSMD pathway targets mRNAs carrying premature stop codons for degradation, therefore, not allowing a truncated protein to be formed (Hug, Longman and Cáceres, 2015). qPCR results shown in *Figure 9E* showed a significant reduction in *lama1* expression in *nl15* mutants with coloboma compared to the wild-type siblings, confirming NSMD.

RNA-seq based mapping using a modification of the Cloudmap mapping pipeline on Galaxy (http://usegalaxy.org/cloudmap; Minevich, Park, Blankenberg, Poole, & Hobert, 2012) showed that the *nl14* mutation is also located at the end of chromosome 24, between 38 and 42Mb (*Figure 9C; n=200*, 100 sibling embryos and 100 embryos with coloboma, from 3 different clutches). Several candidates were identified; however, the standout mutation was located at 418134199mb, a missense mutation, a T-to-C, in *lama1*. This missense mutation results in the substitution of the amino acid at position 124 from Phenylalanine (non-polar) to Serine (polar) in a highly conserved LamNT

domain (*Figure 9D*). It is likely that this mutation generates a hypomorphic Laminin alpha1 protein.

To confirm the SNP in the *lama1*^{nl14} line we used sanger sequencing. By selecting embryos with the coloboma phenotype versus those without, we found that the T-C SNP is present in all seven samples of coloboma mutants, as compared to the siblings where a T-C double peak (heterozygote) was present in two out of seven siblings and a single T peak (wild-type) in four of the seven siblings. However, in one embryo of the sibling batch we found one single C peak (mutant). Given that the coloboma phenotype is not fully penetrant, we presume that the wild-type looking sibling is genetically a mutant (*Figure 9F*).

In order to confirm the *nl14* phenotype was due to the mutation in the *lama1* gene, we performed a complementation test between *nl14* and *nl15* fish. A complementation test shows that if a mutation is on two different genes the progeny receives one copy of a wild-type allele and one copy of a mutant allele and therefore will express a wild-type phenotype. If the mutations are in the same gene, the progeny receive two copies of a mutant allele and therefore display a mutant phenotype. After performing an in cross of heterozygous adults from both lines, the progeny showed a mild coloboma phenotype in an average of 15% of embryos. This percentage and the phenotype were similar to that of the *nl14* allele with no other overt phenotypes (*Figure 9G*). Therefore, from an ENU mutagenesis screen, by WGS, RNA-seq, Sanger sequencing, qPCR and complementation testing we were able to identify mutations in *lama1* as causative of the coloboma phenotype in *nl14* and *nl15* mutants exhibiting coloboma.

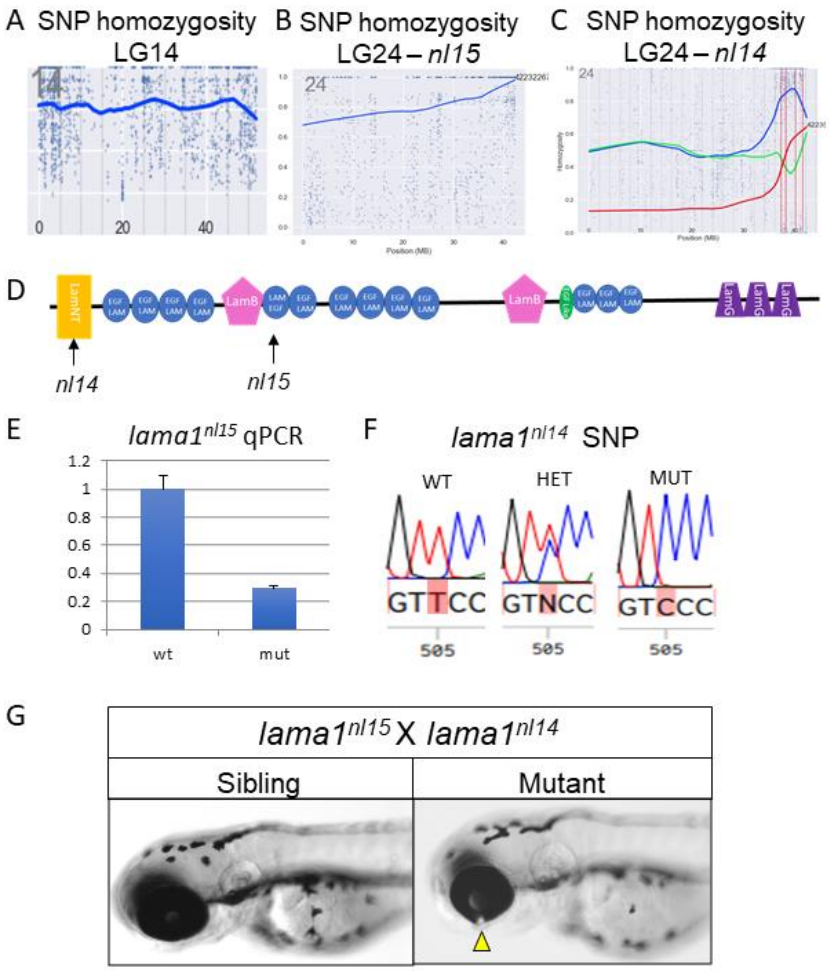

FIGURE 9 BOTH *NL14* AND *NL15* HAVE CAUSATIVE MUTATIONS IN LAMA1

(A, B) Mapping plot of SNP homozygosity across chromosome 14 and 24 showing SNP homozygosity at the end of chromosome 24 in *nl15*. (C) RNA-seq mapping plot showing SNP homozygosity on chromosome 24 in *nl14*. (D) Schematic of the laminin alpha1 protein with arrows indicating the positions of the SNPs in *nl15* and *nl14*. (E) Graph showing the difference in *lama1* expression by qPCR between siblings and mutants in the *lama1*^{nl15}allele. (F) Graphs indicating the peaks at the position of the T-C SNP in WT, Heterozygote (Het) and Mutant (Mut) *lama1*^{nl14}. (G) Complementation test of *lama1*^{nl15} and *lama1*^{nl14} show coloboma (yellow arrow) in 3dpf mutant.

3.3 *laminin alpha1* is important for the maintenance of apico-basal polarity

It has been established that Laminin is essential for the maintenance of epithelial polarity (Martin-Belmonte and Mostov, 2008). Previous studies in *lama1*^{uw1} mutant fish shown that there is a disruption of polarity in the developing eye (Bryan, Chien and Kwan, 2016). We wanted to compare the severity of *nl14* and *nl15* alleles to the *uw1* allele used in these papers. By injecting Pard3:GFP into one cell stage embryos we labelled the apical domains of the neuroepithelial cells. Confocal microscopy at 32hpf showed that both in siblings and mutants there is a clear formation of the apical domain that extends along the lumen of the optic vesicle between the neural retina (NR) and retinal pigmented epithelial (RPE). However, in the mutants there is ectopic expression of Pard3 in both *lama1*^{nl15} (*Figure 10 A, B*; *n = 3*) and *lama1*^{nl14} (*Figure 10 C, D; n = 3*) mutants. The polarity defect is very mild compared to the *lama1*^{uw1} allele and not fully penetrant (Bryan, Chien and Kwan, 2016). Thus, our results showed that, as in previous studies, laminin is an essential component to maintain apico-basal polarity. However, as there is no disruption of polarity specifically in the choroid fissure, we cannot conclude that disruption of the apico-basal polarity in our *lama1* mutants causes coloboma.

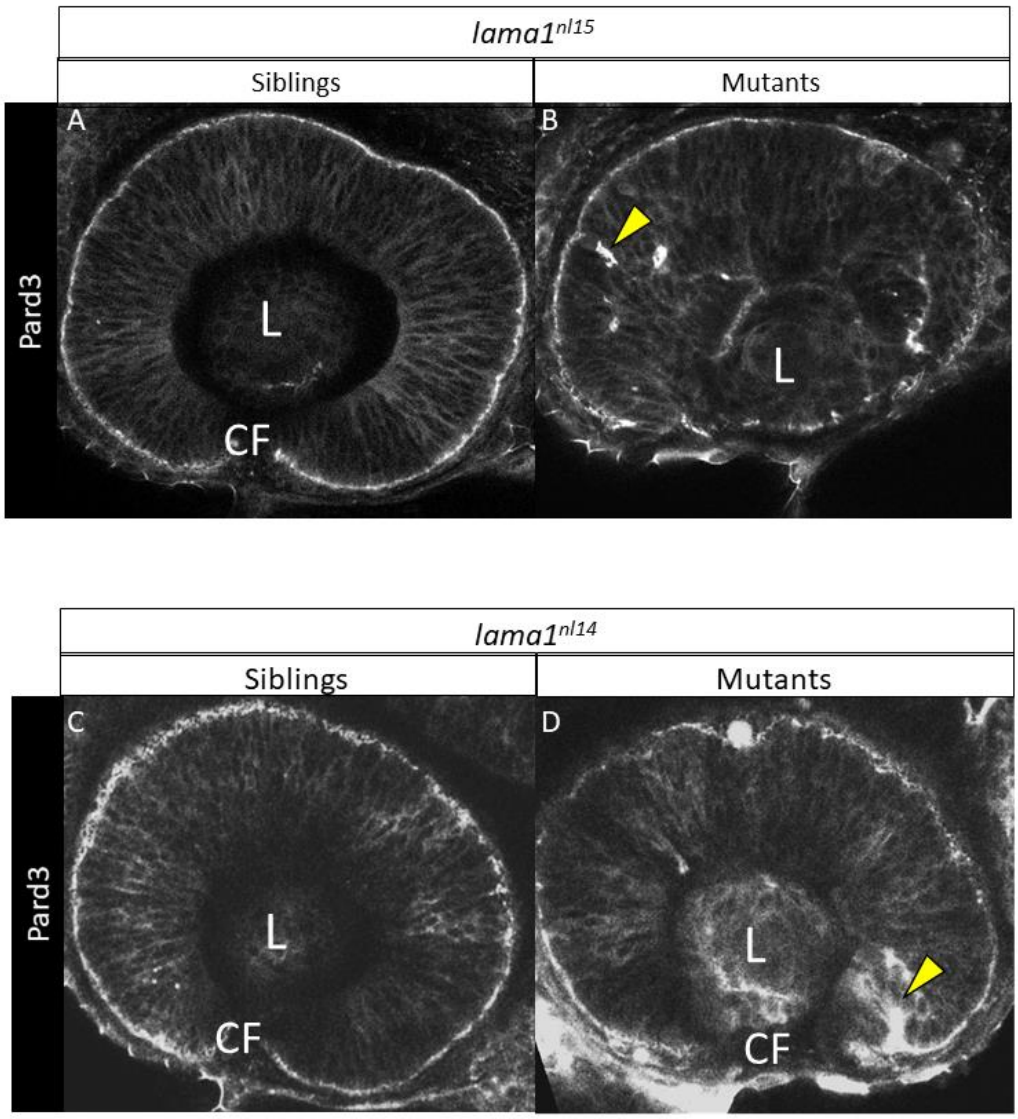

FIGURE 10 APICO-BASAL POLARITY DEFECTS IN *NL14* AND *NL15*

(A-D) Confocal images of the apical marker Pard3 in the eye of 32hpf embryos. (A, C) Sibling of *nl15* and *nl14* and (B) *nl15* mutant and (D) *nl14* mutant showing (yellow arrow) ectopic expression of Pard3.

3.4 Choroid fissure cells of *lama1*^{nl14} mutants are unaffected at the ultra-structural level

A prerequisite for CF fusion is the disappearance of the basal lamina within the fissure (Eckert *et al.*, 2017; Bernstein *et al.*, 2018; Gestri *et al.*, 2018). *lama1*^{nl14} mutants have a mild coloboma phenotype with mild polarity defects making this mutant an excellent tool to study mechanisms of choroid fissure fusion. Thus, we investigated what was happening during the fusion event at an ultra-structural level, performing transmission electron microscopy. Embryos were selected at 62hpf well after 56hpf when fusion is completed in the wild-type embryos and fixed in Karnovsky's fixative (see methods).

We particularly focused on the structural integrity of the basement membrane; the polarity and the morphology of the choroid fissure cells. Choroid fissure cells have been previously characterised as RPE like but with a different gene expression profile (Richardson *et al.*, 2019).

The CF cells lines up along the opposing lips of the choroid fissure during fusion (*Figure 11 A, B* labelled CFC), with no obvious difference in size or shape of the cells in comparing wild-type siblings to mutants. Given that fusion is taking place in the analysed mutants we cannot make any conclusion on whether there is any difference at the ultra-structural level (*Figure 11B*). In order to understand how fusion is compromised in the *nl14* allele we would have to select embryos at a later stage when the coloboma phenotype is clear.

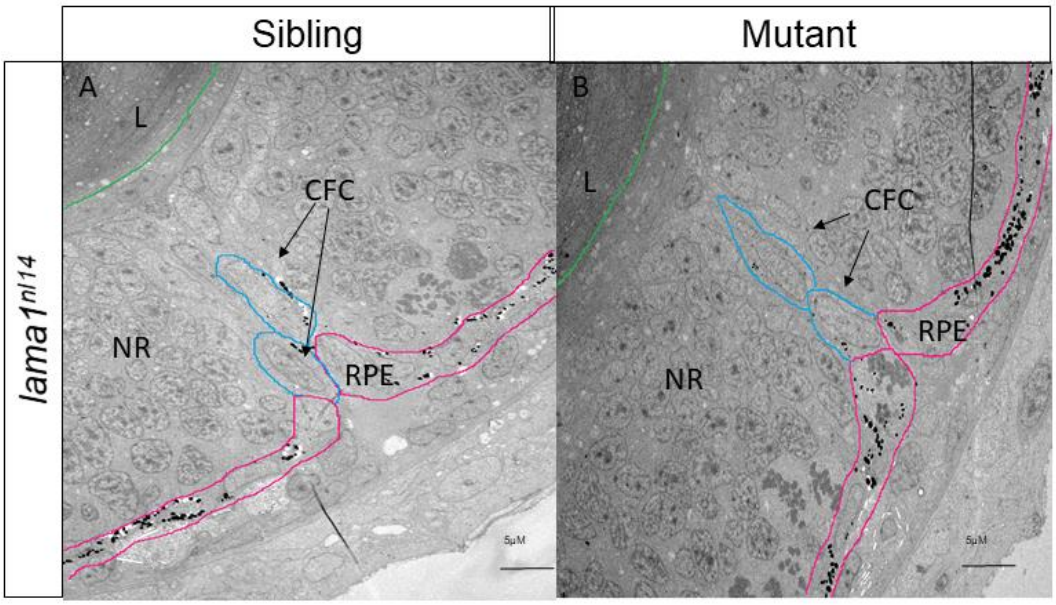

FIGURE 11 THE CHOROID FISSURE AT THE ULTRA-STRUCTURAL LEVEL IN *LAMA1*^{NL14}

(A) A wild-type sibling showing the choroid fissure cells lined up along the fissure (labelled CFC in blue) and the RPE cells in magenta. (B) A mutant showing CFC (blue) lined up along the fissure and the RPE cells highlighted in magenta.

3.5 *laminin alpha1* is important for the development of the hyaloid vasculature

It has been established that disruptions to the hyaloid vasculature can lead to failure in choroid fissure fusion (James *et al.*, 2016). Previous studies in *lama1* morphants suggest that without properly functioning *lama1,* the hyaloid vasculature does not form properly (Semina *et al.*, 2006). Therefore, we decided to investigate if a similar observation could be seen in the *lama1*^{nl14} allele. As the *lama1*^{nl15} phenotype is too severe and the lens extrusion makes imaging particularly difficult, we did not use this allele for further experiments.

The *lama1*^{nl14} line was crossed with a transgenic line, in which the GFP labels the vasculature in zebrafish embryos; Tg(kdrl:eGFP^{s843}). We selected embryos that show a coloboma phenotype and their wild-type siblings at 72hpf and performed immunohistochemistry against GFP.

In wild-type siblings, the hyaloid artery can be seen entering the choroid fissure, the three distinct branches of vessels; nasal radial vessel (NRV), dorsal radial vessel (DRV) and ventral radial vessel (VRV) connected by the superficial annular vessel (SAV) and the exit of the hyaloid vein through the choroid fissure (*Figure 12A*; James et al., 2016; Kaufman et al., 2015; Weiss et al., 2012). In the *lama1*^{nl14} mutants, the HA enters as normal and does not appear to have any defect in size as has previously described in other coloboma mutants (Weiss *et al.*, 2012; James *et al.*, 2016) and the three branches are all fully formed (*Figure 12B*). However, despite being able to visualise the hyaloid vein, which also does not appear to have any obvious disruption, a lack of temporal vasculature was observed in two out of six mutants (*Figure 12B*).

This data suggests that there is variable disruption or an arrested development of the superficial annular vessel. However, as this is not present in all mutants with coloboma, we can conclude that the vasculature defect is not causing the coloboma phenotype.

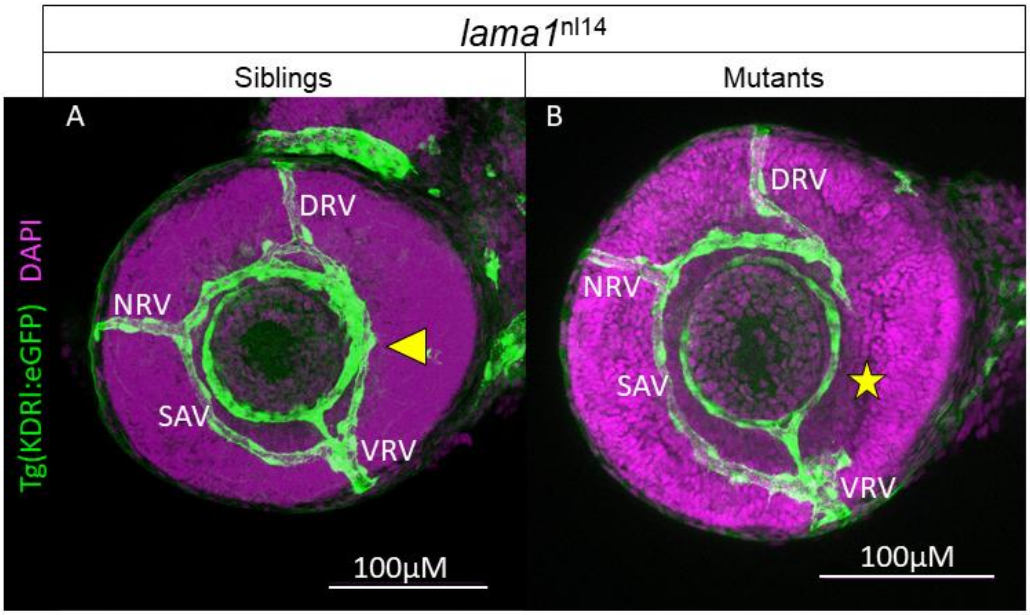

FIGURE 12 CONFOCAL IMAGES OF THE HYALOID VASCULATURE IN THE EYE

A lateral view in *lama1*^{nl14} siblings (A) and mutants (B). Tg(kdrl:eGFP) labelling the nasal radial vessel (NRV), dorsal radial vessel (DRV) and ventral radial vessel (VRV) connected by the superficial annular vessel (SAV) is shown in green and DAPI in magenta.

3.6 Photoreceptors are unaffected in *lama1*^{nl14}

lama1 mutants (*bal*^{a69}) with severe lens defects showed ectopic localization of photoreceptor cells in the neural retina (Semina *et al.*, 2006). This phenotype is independent of the lens phenotype; indeed, in lens ablated control embryos the photoreceptor layer appears normal in the differentiated retina. This study concludes that the disruption to the photoreceptors is therefore due to the *lama1* mutation and not the result of the loss of the lens structure (Semina *et al.*, 2006). Therefore, we decided to compare the *nl14* allele, in which lens is not compromised, to this study.

lama1^{nl14} sibling and mutants selected for the presence of a coloboma phenotype were fixed at 5dpf and cryosectioned (*n*=12 sibling and *n*=12 mutants). Embryos were immunolabelled with Zpr1 (which labels the cones in the photoreceptor layer) and imaged via confocal microscopy. We were able to visualise the fully formed and differentiated photoreceptor layer as well as the outer segments of the cones. We did not observe any defects in localization of Zpr1 expression in the fully differentiated eye. The layer appears normal even in the ventral retina, around the point of the coloboma phenotype (*Figure 13 A, B*). High magnification of the cones showed no major differences between wild-type and mutants (*Figure 13 6A', B*).

In order to analyse the outer segment of the cones with higher resolution, we performed plastic sections. Sections were stained with Sytox Green and Bodipi – which label the nuclei and outer segment, respectively. As observed in the cryosections, the photoreceptor layer is unaffected even around the point of the coloboma phenotype in the mutant compared to its wild-type sibling (*Figure 13 C, D*, *n* = 1 sibling and *n* = 1 mutant). Moreover, no obvious difference in the outer segments in siblings compared to mutants were observed (*Figure 13 6C', D'*).

In conclusion, we showed that the photoreceptor cells are normal in both siblings and mutants.

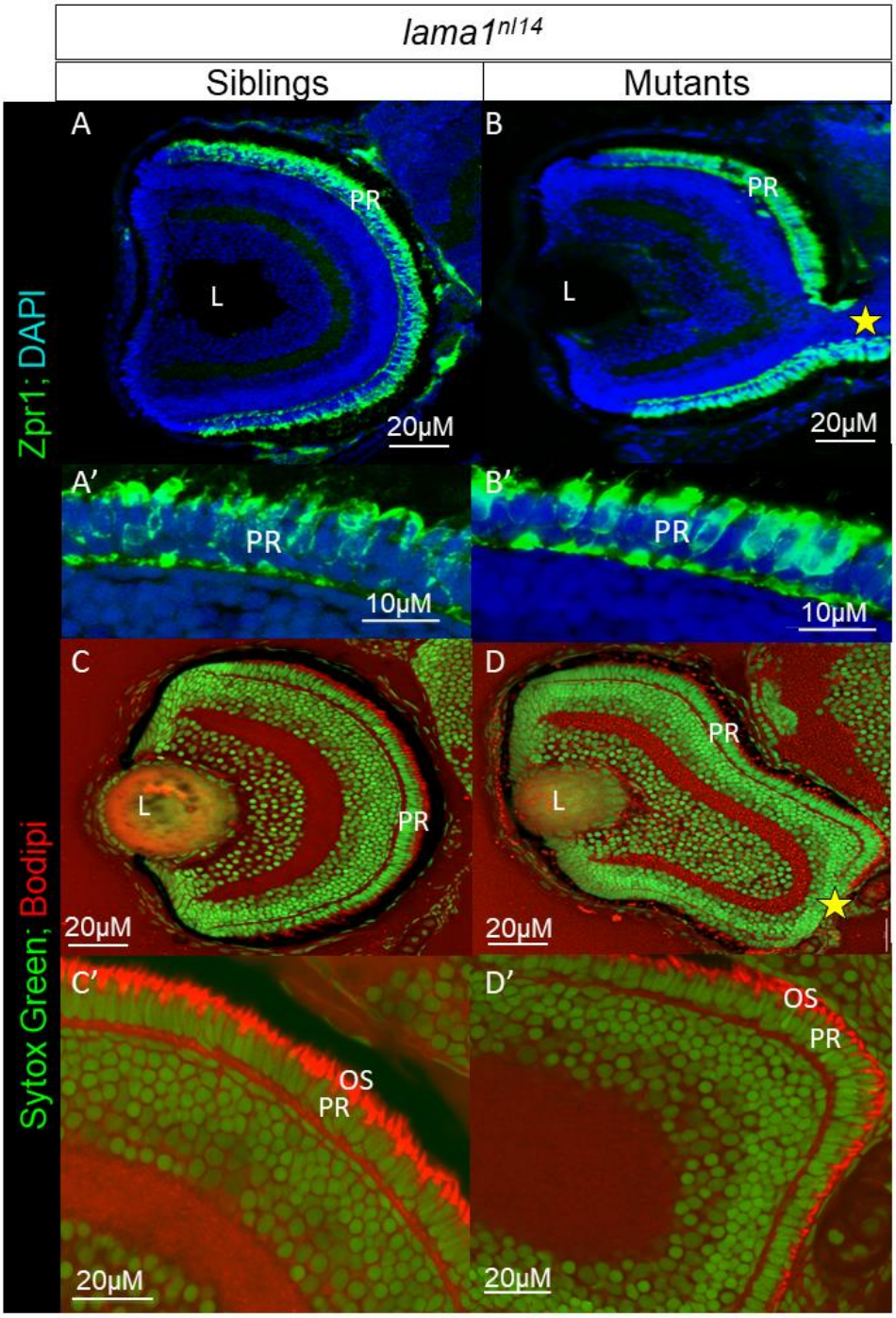

FIGURE 13 IMAGES OF PHOTORECEPTORS IN *LAMA1*^{NL14}

(A, A') Sibling and (B, B') mutant stained with Zpr1 (green) and DAPI (blue). (A') and (B') show magnified (x63) images with the lens marked by an L and photoreceptor by PR. The yellow star indicates the extrusion of the neural retina. (C, C') Sibling and (D, D') mutant of plastic sections stained with sytox green (green) and bodipi (red) to highlight outer segment (OS) with the yellow star indicating the extrusion of the neural retina. (C', D') Magnified images of the outer segment.

3.7 *lama1*^{nl14} mutants with coloboma have severe vision loss

The phenotype in patients with coloboma can be varied. For example, patients with a superficial coloboma can see as normal, however, coloboma of the optic stalk and nerve will cause blindness (ALSomiry, Gregory-Evans and Gregory-Evans, 2019). We therefore wanted to determine if *lama1*^{nl14} mutants with coloboma replicate that of humans and suffer from vision loss.

We decided to use the OKR set up to assess visual function in the *nl14* coloboma line as described in the introduction and shown in *Figure 14A*. Black and white stripes were projected onto the drum at different speed, spatial frequency and contrast as shown in *Figure 14B*. Larvae were selected on their phenotype, wild-type versus colobomatous and the larvae with coloboma were further scored on the laterality of their phenotypes; bilateral, monolateral left and monolateral right and their severity; subtle, mild and severe as shown in *Figure 14C*. The eye movements are tracked as shown in *Figure 14D* and analysed via custom matlab scripts.

In general, *lama1*^{nl14} mutants exhibiting coloboma suffer from severe vision loss in all differing conditions of spatial frequency, contrast and speed compared to the wild-type siblings as shown in *Figure 15A, A'' and A'''*. However, as wild-type larvae also struggle to discriminate the stimuli as the conditions become more challenging, we decided to focus on the comparison of wild-type versus coloboma in what we termed the 'easiest trial' i.e. the trial that has the lowest spatial frequency, highest contrast and lowest speed (highlighted in yellow in *Figure 14B*), where we know that wild-types always respond well to this trial, allowing us to determine if the laterality or severity of coloboma has an impact on vision loss.

We first observed that the more severe the coloboma the more severe the vision loss (*Figure 15B*), showing that the severity of the coloboma has an effect on visual function. To further address if the presence of the coloboma is the only cause for vision loss we compared both eyes in larvae with monolateral coloboma. By comparing the coloboma affected eye to the wild-type

contralateral eye we were able to discover that even though a decrease in visual performance can be noted in the colobomatous eye, the contralateral wild-type eye is also affected (*Figure 15C*).

Thus, our results suggest that *lama1*^{nl14} larvae have visual impairment that is aggravated but not exclusive to the presence of a coloboma phenotype.

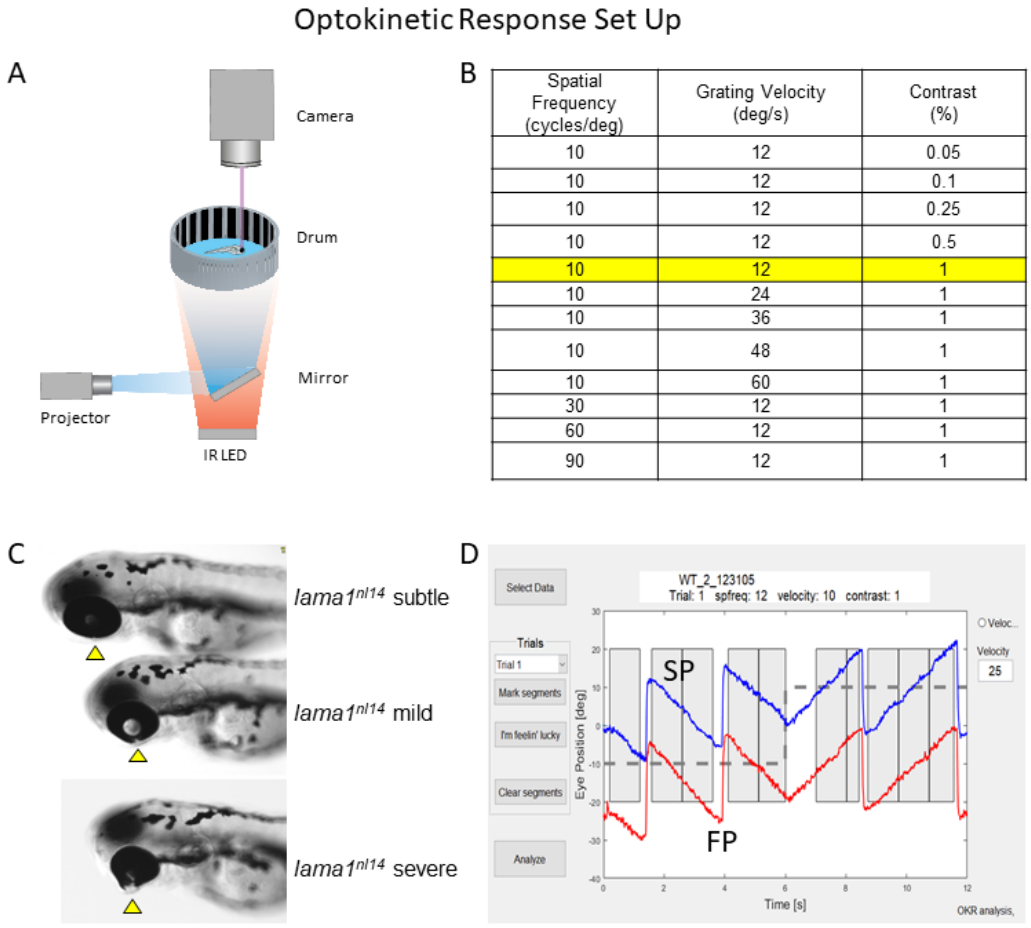

Spatial Frequency (cycles/deg)	Grating Velocity (deg/s)	Contrast (%)
10	12	0.05
10	12	0.1
10	12	0.25
10	12	0.5
10	12	1
10	24	1
10	36	1
10	48	1
10	60	1
30	12	1
60	12	1
90	12	1

FIGURE 14 OPTOKINETIC RESPONSE SET UP

A schematic of the set-up of the OKR method adapted from Joanna Lau and *Henriques, Rahman, Jackson, & Bianco, 2019*. The visual stimuli are presented from the computer via the projector onto a drum. The larva is embedded in 2% low melting agarose which has been cut away from the eyes to allow them to move. A camera above the larva tracks the eye movement. (B) The trials used during this experiment with the 'easiest trial' highlighted in yellow. (C) The phenotypes with the yellow arrow indicating the coloboma and their score used during this experiment. (D) An example of the eye movement data produced using this methodology. The slow response phase (SP) is followed by a fast resetting saccade (fast phase, FP).

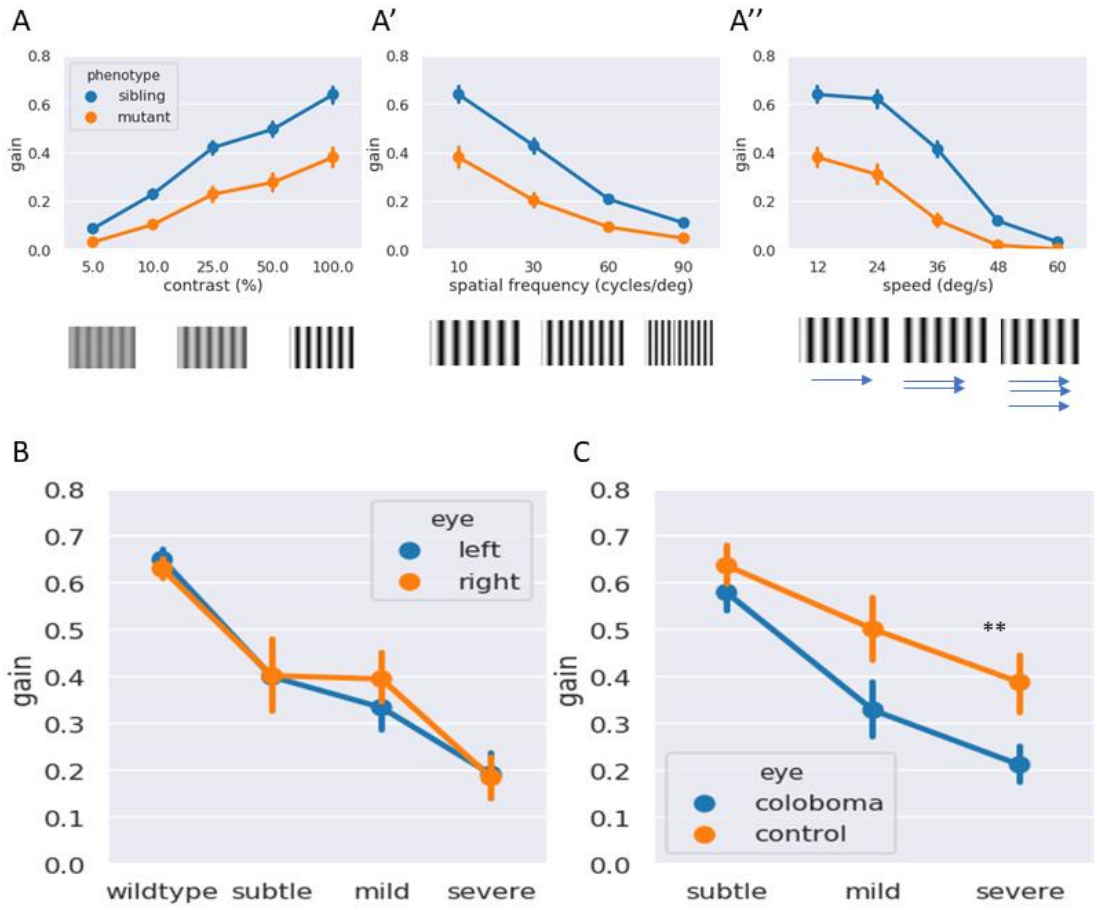

FIGURE 15 OPTOKINETIC RESPONSE RESULTS

(A, A' and A''') Graphs showing the difference between mutant larvae with coloboma versus wild-type siblings. The mutants always have a decreased response across all trials. (B) A graph showing the difference in response to the 'easiest trial' in the different severities of coloboma. The more severe the coloboma the more severe the vision loss. (C) A graph showing the difference between a coloboma affected eye versus it's contralateral wild-type eye in monolateral coloboma affected larvae using the 'easiest trial'. Bands show the confidence intervals (95%) and there is a significant difference (*p=<0.01*) found in severe coloboma versus subtle coloboma found by t test.

3.8 Retinal projections leaving the eye and entering the optic tecta are misguided in *lama1*^{nl14} mutants

The coloboma phenotype has been associated with retino-tectal projection defects (Semina *et al.*, 2006). However, a clear correlation between coloboma phenotype, retino-tectal projection and vision loss has not been reported yet. Disruption of laminin in *lama1* morphants causes axonal guidance defects in zebrafish (Semina *et al.*, 2006), thus we decided to investigate the retino-tectal projections in *lama1*^{nl14} mutants.

In order to visualise RGC projections, we crossed *lama1*^{nl14} line with a transgenic line in which GFP labels the retinal ganglion cells and their projections (RGCs); Tg(ath5:eGFP^{rw021}) and performed an immunohistochemistry against GFP at 5dpf. In wild-type siblings the RGC projections crossed at the optic chiasm to project to the contralateral tectum (*Figure 16A, A'*). In the mutants with coloboma (*n=2*), the phenotypes are variable, with different severities of misguidance of projections. We observed lack of crossing at the optic chiasm, projections to the telencephalon and reduction in ipsilateral and contralateral projections (*Figure 16B, B'*).

Next, we wanted to correlate OKR results with RGC defects. Given that the OKR assay was carried out in embryos that where not transgenic for the retinal ganglion cells marker, after performing OKR, five-day old larvae where labelled with DiI and DiD crystals to label the retinal projections as they leave the eye and enter the optic tecta. The analysis (*n=8* siblings and *n=8* mutants) shows that the more severe coloboma phenotypes have more severe misguidance issues and that even in mild cases there are misguided axons. However, in the subtle coloboma phenotype, as well as the contralateral wild-type looking eye, the RGC projects correctly to the contralateral tectum (*Figure 16C, D*).

These results showed that *lama1*^{nl14} is required for proper axonal projections. Whilst it seems there is a correlation between coloboma and misguided axons and vision loss, more numbers are needed to absolutely confirm this theory.

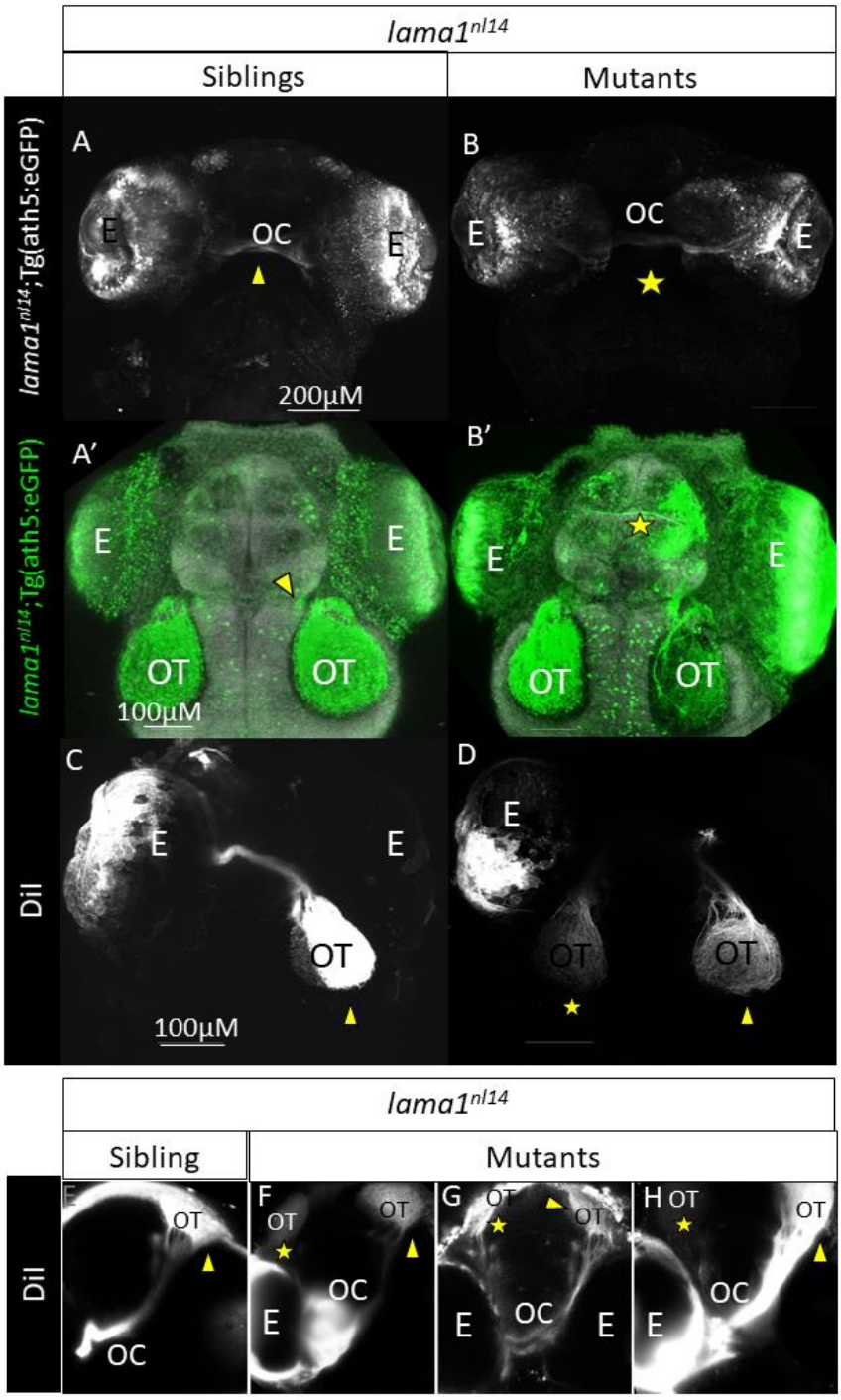

FIGURE 16 RETINO-TECTAL PROJECTIONS IN *LAMA1*^{NL14} MUTANTS

(A, B) Ventral view of a sibling (A) showing RGCs exiting the eye (E) and crossing at the optic chiasm (OC) and a mutant (B) lack of crossing in *lama1*^{nl14} mutant with severe coloboma, highlighted by the yellow star. (A', B') Dorsal view of the previously described sibling (A') and mutant (B') showing the pathway of the projections to the optic tecta. Star in (B') points to the misguided RGCs exiting the eye. (C-H) Dorsal view of siblings (C, E) showing RGC projection to the contralateral optic tectum. *lama1*^{nl14} mutants with (F) severe coloboma, (D, G) mild coloboma and (H) subtle coloboma that show normal contralateral projection (arrow) as well as the misguided ipsilateral projection (star).

3.9 *Clusterin* gene expression is increased in the lens of *lama1*^{nl14} mutants

RNA seq was performed on RNA extracted from whole embryos of 3dpf sibling and mutant embryos presenting with coloboma. From the data we identified a number of genes that were up or down regulated in the *lama1*^{nl14} mutants (*Figure 17A*). We decided to validate the RNA seq by performing an *in situ* hybridisation (*in situ*) of selected genes and visualising any spatial differences in gene expression in the embryos. We performed the *in situ* at 3dpf to correlate with the time point of the RNA seq data.

Of the seven genes analysed, *clusterin* showed increased expression in the lens of *lama1*^{nl14} mutants compared to the wild-type siblings (*Figure 17 B-C'*). The increased expression was found in 10/13 mutants – 8 had a monolateral expression, 2 bilateral and the 3 remaining mutants had no increased expression and looked like their wild-type siblings. This replicates what we have seen previously with incidences of bilateral and monolateral colobomas and a non-penetrant phenotype. As *clusterin* is known to be a regulator of cell death it opens the possibility that the increased expression is due to an increase in cell death in the lens. However, as there is expression in the midline cells and we know that these are not dying, we would have to confirm whether there is an increase in cell death by performing a TUNEL assay. This allows us to hypothesise that a defect in the lens may also contribute to the vision loss observed with the OKR.

A

ENSDARG	log2FoldChange	pvalue	padj	Gene name	Chromosome	Up/Down
ENSDARG00000061417	0.750981	6.62E-12	5.85E-08	nub1	24	Down
ENSDARG00000059128	0.650039	1.88E-13	4.99E-09	uqcrh	6	Down
ENSDARG00000087446	0.628172	9.03E-09	4.79E-05	mmd2a	3	Down
ENSDARG00000044545	0.619387	1.01E-12	1.33E-08	zgc:77262	21	Down
ENSDARG00000103498	0.563683	6.93E-09	4.6E-05	epd	5	Down
ENSDARG00000094048	0.523463	6.7E-08	0.000296	si:dkey-224b4.5	24	Down
ENSDARG00000031240	0.517355	2.22E-06	0.006525	kidins220a	17	Down
ENSDARG00000038228	0.488308	3.35E-06	0.008869	sepw2a	3	Down
ENSDARG00000093671	0.459382	4.07E-05	0.077072	BX001030.1	24	Down
ENSDARG00000012688	0.429561	1.65E-05	0.036464	eif1b	19	Down
ENSDARG00000086586	0.426192	4.07E-07	0.001542	BX323854.3	24	Down
ENSDARG00000042613	0.351707	2.54E-05	0.05173	crp3	24	Down
ENSDARG00000022951	-0.41416	1.78E-06	0.005901	pth2	17	Up
ENSDARG00000010434	-0.47051	1.37E-05	0.032922	clu	20	Up

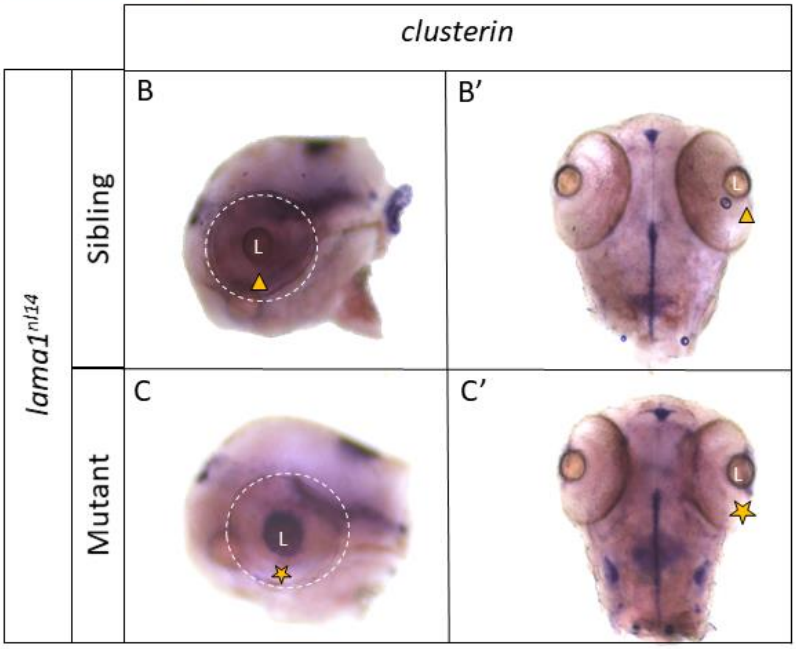

FIGURE 17 UP AND DOWN REGULATED GENES FROM RNA SEQ IN *LAMA1*^{NL14}

(A) Table of significantly up and down regulated genes in *lama1*^{nl14}. (B-C') *clusterin* expression in sibling lateral view found in the lens (L) (B) and dorsal view (B'). Increased *clusterin* expression in mutant lateral view (C; yellow star) and dorsal view (C'; yellow star).

3.10 Generating a choroid fissure transgenic line

To date, there are not tools to exclusively visualise choroid fissure cells. Thus, to determine how the choroid fissure cells impact fusion and their fate once fusion has taken place, new tools are required.

In order to generate a transgenic line that is expressed only in the choroid fissure and that will allow us to manipulate the fate of the choroid fissure cells with the UAS/Gal4 system, we took advantage of the CRISPR/cas9 technique which allows us to knock in a construct that contains Gal4:GFP as shown in the diagram *Figure 18A*.

We chose the gene *netrin1a* as our target as *netrin1a* is known to be expressed only in the choroid fissure cells from 36hpf (Bibliowicz, Rachel K Tittle and Gross, 2011; Gestri *et al.*, 2018; Richardson *et al.*, 2019).

In the first attempt of injections, we appeared to have found an F1 founder that had germ line transmission (*Figure 18B*). However, using the genomic DNA from labelled embryos and running a PCR with *netrin1a* and Gal4 primers, no bands could be seen, and it appeared that this was not a true founder (*Figure 18C-E*). This approach has been very time-consuming and resulting in only one potential founder which turned out not to be true. Due to the low efficiency of our initial approach, we have decided to pursue this further using commercially purchased guide RNAs and cas9 protein. As this is still in the testing phase, we have no conclusion to make on this part of the project.

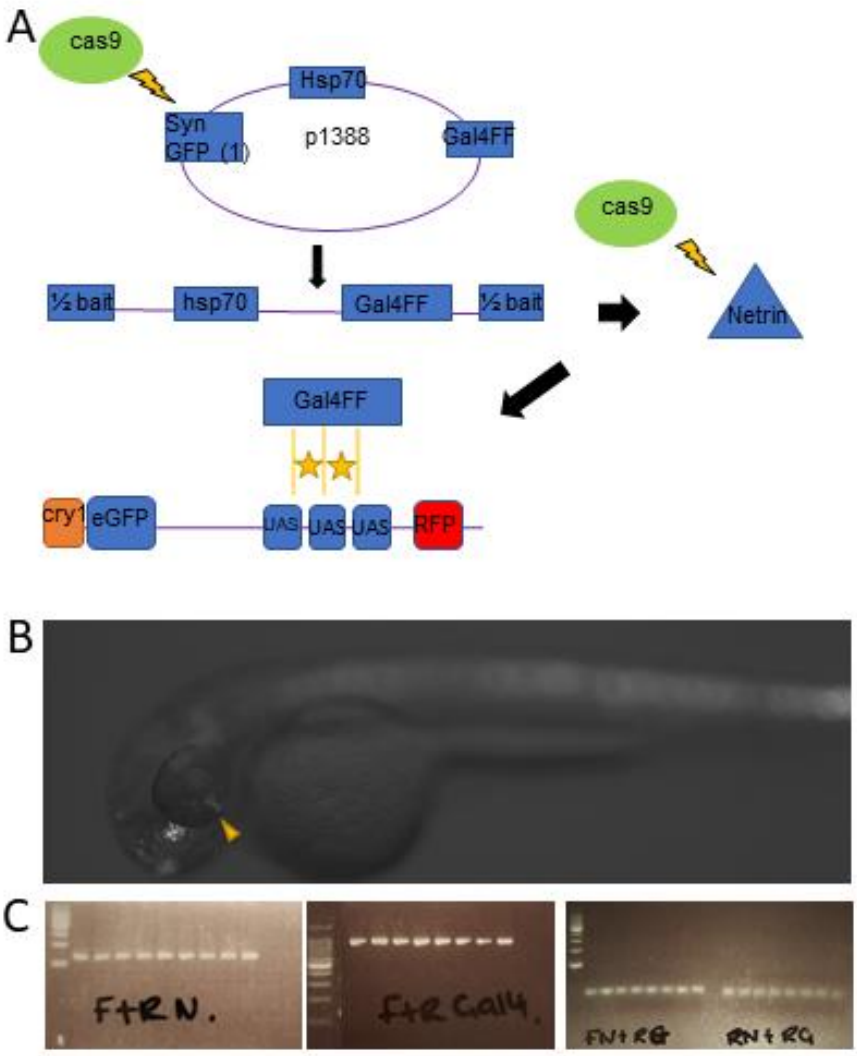

FIGURE 18 GENERATING A NEW CHOROID FISSURE LINE

(A) A schematic showing how the construct will be inserted into the *netrin1a* gene. (B) Potential expression of *netrin1a*. Gel electrophoresis images showing bands for *netrin1a* control (C), Gal4 control (D) and lack of bands in combination of *netrin1a* and Gal4 in potential founder (E).

4 Discussion

In this study, we have characterized two zebrafish mutants with different severities of coloboma and vision loss. The causative mutations in both these lines were mapped to *laminin alpha1*. *lama1* is a well-studied gene and previous studies have shown phenotypes such as lens extrusion, hyaloid vasculature, polarity, axonal pathfinding and body axis defects (Semina *et al.*, 2006; Zinkevich *et al.*, 2006; Pathania, Semina and Duncan, 2014). However, these studies have never shown or described their mutants as having coloboma, therefore, we have characterised a new phenotype to be associated with this gene.

4.1 *lama1* as a risk factor for coloboma

The list of genes implicated in eye development defects is rising but only accounts for a minority of cases of coloboma. We understand even less about the highly variable penetrance and expressivity of coloboma phenotypes. It is even common for left and right eyes to express very different phenotypes despite carrying the same genetic lesions both in model systems as well as human patients (Kathleen A. Williamson and FitzPatrick, 2014; Cavodeassi and Wilson, 2019). It is becoming clear that it is not individual genes but a combination of risk factors that are causing phenotypes (Cavodeassi and Wilson, 2019). Eye morphogenesis is known to be a robust system due to genetic compensation and robustness of developmental and molecular pathways (Cavodeassi and Wilson, 2019). In a recent study in a *tcf7l1a* mutant, homozygous embryos showed a reduced size in the eye field but would still form a normal sized eye by 5dpf, however, this mutation sensitises the system and by mutating other genes, the eyes do not form and the embryos display anophthalmia (loss of eyes) (Young *et al.*, 2019).

Here, we showed that the *nl14* mutation in *lama1* lead to a non-fully penetrant coloboma phenotype. In absence of additional stressors, coloboma is rare and usually unilateral whereas at a higher, stress-inducing temperature,

penetrance of coloboma is found in 55% of mutants and is often bilateral. *Laminin beta1* (*lamb1*) and *laminin gamma1* (*lamc1*) mutants (which contribute to form the laminin-111 heterotrimer) can also exhibit coloboma in zebrafish, suggesting a redundant role for laminin genes in choroid fissure closure. In the study of *bal*^{tp82}, the authors suggested that *lama5* could be compensating for the loss of *lama1* (Biehlmaier, Makhankov and Neuhauss, 2007).

We propose that disrupted *lama1* function constitutes a risk factor and *lama1* mutants can be used as a sensitized genetic background in which to identify other genes that, when mutated in combination with *lama1*, lead to severe eye malformations. One obvious candidate is *netrin1*, another extracellular matrix component that has been implicated in coloboma both in chicks and zebrafish (Hardy *et al.*, 2019; Richardson *et al.*, 2019). As new data from the 100K genome project begins to be released, it will be interesting to look for SNPs that are present in combination with *lama1* and create models/networks of the candidate genes that sensitise the system. As choroid fissure fusion is such a complex event, we could start to group genes into which part of the fusion process they might participate. This will help to get a better understanding of how each step of fusion proceeds and how robust the system is.

4.2 Mild apico-basal polarity defects in *lama1*^{nl14} *and lama1*^{nl15} embryos

Apico-basal polarity is essential for the cell movements that drive optic cup morphogenesis (Hehr, Halabi and McFarlane, 2018). Indeed, if both components are disrupted, as in the case of *traf4a* (a component of tight and adherens junctions) and laminin1, this results in optic vesicle defects. However, despite this early requirement subsequent events of eye morphogenesis and choroid fissure fusion might not be affected (Hehr, Halabi and McFarlane, 2018).

Optic cup morphogenesis occurs normally in the *lama1*^{nl14} mutants (data not shown) and the temporal and nasal margins of the choroid fissure become

properly apposed but choroid fissure fails to fuse. This suggests that the phenotype is not a secondary consequence of defects in the optic cup formation but a failure of the fusion process itself. As we know that prior to fusion, apico-basal polarity in the choroid fissure needs to be rearranged and basal lamina degraded, we investigated whether we could find any polarity defects in the choroid fissure of both *lama1*^{nl14} and *lama1*^{nl15}. Moreover, polarity defects were described in *lama1*^{uw1} allele (Bryan, Chien and Kwan, 2016). Both *lama1*^{nl14} *and lama1*^{nl15} have mild polarity defects, milder than the previously described *lama1*^{uw1} allele and the polarity defects were not seen in the choroid fissure specifically, suggesting that polarity defects are not contributing to coloboma.

4.3 *lama1* could contribute to vasculature defects in zebrafish

Vasculature forms just prior to fissure fusion and it has been shown that signalling from the hyaloid vasculature facilitates basal membrane breakdown during CF fusion, linking vasculature defects to coloboma (Weiss *et al.*, 2012; James *et al.*, 2016). Vasculature mutants such as *LIM domain only 2* (*lmo2)* have dilated vessels that stop the nasal and temporal retina to come together to allow fusion to occur (Weiss *et al.*, 2012). Moreover, laminin and ECM components are required for hyaloid vasculature development and differentiation (Alvarez *et al.*, 2007). Mutations in numerous genes that are crucial for ECM composition display vasculature defects including arrested development of the hyaloid vasculature, lack of branching vessels and issues with vessel size (Alvarez *et al.*, 2007). Further, there are a range of vasculature phenotypes associated with *lama1* disruption. *lama1* morphants show disruption in the formation of the hyaloid vasculature (Semina *et al.*, 2006). Moreover, a further study in a *lama1* mutant, *arl* (*arrested lens*) shows that there is a complete lack of intraocular vasculature by 3dpf (Alvarez *et al.*, 2007) and another review of laminins in vascular development mentions that there are no branching of capillaries from the endothelial cells at 24hpf (Edwards and Lefebvre, 2013). Furthermore, this link of *lama1* to retinal vasculature can also be seen in mice. It was found that there is no disruption to initial

differentiation or migration of endothelial cells and the deep and intermediate vascular plexi form as normal in *Lama1* mouse mutants compared to their wild-type siblings (Edwards and Lefebvre, 2013). However, as development continues the endothelial cell migration stalls and therefore results in a lack of superficial vasculature determining the importance of *lama1* in cell migration (Edwards and Lefebvre, 2013). Moreover, from this study they also suggest the similarities of the *lama1* vascular phenotype to human retinal disorders. The two disorders; Persistent Foetal Vasculature (PFV) and Knobloch Syndrome, both show failure of the regression of the hyaloid vasculature (Goldberg, 1997; Edwards and Lefebvre, 2013). This failure can result in retinal detachment and therefore blindness (Goldberg, 1997; Edwards and Lefebvre, 2013). Therefore, it was suggested that *lama1* be added to the screening list for patients with PFV or Knobloch Syndrome.

Even though we observed a lack of temporal vasculature in some mutants, the vessels that enter through and exit the fissure, appear organized and normal. This data suggests that the coloboma in *lama1*^{nl14} is not caused by any vasculature defect and that the lack of temporal vasculature could be either a delay in development or an additional phenotype.

To further investigate this hypothesis, it would be necessary to repeat this at a later time point and in the *lama1*^{nl15} allele. It would be interesting to see if we see similar results to those previously described (Semina *et al.*, 2006; Alvarez *et al.*, 2007; Hartsock *et al.*, 2014). This would confirm a role for *lama1* in vasculature development.

4.4 *lama1* mutants with and without coloboma have compromised vision

Vision loss has previously been described in *lamb1* and *lamc1* mutants and at the lowest contrasts in *bal*^{tp82} mutants (Biehlmaier, Makhankov and Neuhauss, 2007). The conclusion from this paper states that the photoreceptor layer is missing in *lamb1* and *lamc1* fry which makes these mutants blind, whereas in *bal*^{tp82} the vision loss is due to the defective lens morphology and disrupted GCL. They suggest that as different laminin isoforms are present in different areas of the eye, the defects in each case are specific to each laminin isoform (Biehlmaier, Makhankov and Neuhauss, 2007).

We wanted to test our model for vision loss to be able to replicate the condition in humans and to compare *lama1*^{nl14} to the previously studied *bal*^{tp82} (Biehlmaier, Makhankov and Neuhauss, 2007). We determined that there is vision loss in *lama1*^{nl14} mutants. To explore this further, we selected the 'easiest' trial as a base and analysed the data of different severities of coloboma and bilateral versus monolateral. We determined that there is a correlation between the severity of coloboma to the severity of vision loss.

In monolateral coloboma larvae, we compared the colobomatous eye to the wild-type looking contralateral eye to investigate if the wild-type eye is able to respond as well as a wild-type sibling. The results show that this is in fact not the case and the wild-type looking eye does not respond as well as sibling eyes but does not have such a severe deficiency as its contralateral colobomatous eye. This could be due to the fact that the eye movement in zebrafish are conjugated. Zebrafish as well as many lateral eyed animals display yoked eye movements: the two eyes move in the same direction and the timings of binocular saccades are synchronous (Beck *et al.*, 2004; Huang and Neuhauss, 2008). Such movements are required to maintain the spatial relationship between the two visual fields (Voss and Bischof, 2009).

Monocular stimulation experiments were able to unveil the extent of independent eye movement in different teleost species at different developmental stages (Beck *et al.*, 2004). In zebrafish, at the early larva stage,

the same stage tested in our experimental approach, the monocular stimulated eye viewing the usual rotating stripe pattern respond similarly to the binocular eye even if the contralateral eye, stimulated with a *ganzfeld* (a featureless visual surrounding) performs quite badly. This shows that the eyes move independently of each other. The eye movement became less decoupled in older larvae (Beck *et al.*, 2004). Thus, we will be performing a similar experiment where we project a *ganzfeld* field to the coloboma eye and a rotating stripe pattern to the wild-type looking eye and vice versa in order to confirm that in our experimental condition the wild-type looking eye in *lama1*^{nl14} mutant is not responding due to the mutation in *lama1* and not because it is 'following' the contralateral coloboma eye.

4.5 Misguided retinal projections in *lama1*^{nl14} mutants are a contributing factor to vision loss

Laminin is known to play a key role in axon guidance in different parts of the nervous system including the eye (Semina *et al.*, 2006; Biehlmaier, Makhankov and Neuhauss, 2007; Varshney, Hunter and Brunken, 2015). In *bal* mutants, it was found that RGC axons tend to be misguided within the eye and are disorganized instead of growing radially inward (Karlstrom *et al.*, 1996). When they do exit the eye they tend to project ipsilaterally as well as contralaterally and even anteriorly toward the telencephalon (Karlstrom *et al.*, 1996). Thus, we analysed RGC projections in *lama1*^{nl14} mutants (Karlstrom *et al.*, 1996; Semina *et al.*, 2006; Biehlmaier, Makhankov and Neuhauss, 2007). Our data shows axonal misguidance in *lama1*^{nl14} mutants. Like for *lama1* morphants and *bal* mutants, the RGC axons make very specific guidance errors; while the projections exit the eye correctly, they make mistakes at particular locations, projecting either to the ipsilateral, as well as the contralateral optic tecta, or to the telencephalon. We considered the possibility that the degrees of vision loss correlate with RGC defects and that RGC projection defects might be present even in mutant eyes that don't have a coloboma. From the data, we could conclude that misguided axons are not the only cause of vision loss in *lama1*^{nl14} mutants.

Moreover, normal apico-basal polarity is essential for the formation and guidance of the RGC axons. RGCs differentiate with the neuroepithelium and axons are known to always protrude from the basal side of the cell (Zolessi *et al.*, 2006). The dendrites polarize apically and grow towards the IPL, whereas the axons extend basally along the retina where they collect at the optic disc and exit via the optic nerve (Randlett, Norden and Harris, 2011). In mutants that have disruption to apical junction complexes such as *nok*, polarity in the neuroepithelium is disrupted (Zolessi *et al.*, 2006; Randlett, Norden and Harris, 2011). In these mutants the RGCs are not in the correct position and lie on the apical side of the neuroepithelium. Not only are they incorrectly positioned but they also show a reverse in cell orientation (Zolessi *et al.*, 2006). However, despite this defect in orientation the axons are able to grow towards and find the optic nerve just in a slower and more erratic manner (Zolessi *et al.*, 2006). Laminin-1 is required for dendrite outgrowth (Long and Huttner, 2019) and from our data we know that the RGCs in *lama1*^{nl14} are mislocalized. Given the very mild polarity defects observed in this allele, it seems unlikely that the RGCs pathfinding defects observed are a consequence of disrupted apico-basal polarity.

4.6 RNA seq data revealed genes of interest that may contribute to the *lama1*^{nl14} allele

From the RNA seq results of *lama1*^{nl14}, we found two genes that were upregulated and seven that were down regulated in the mutants. We performed *in situ* hybridisation on 3dpf embryos to investigate whether this could confirm the RNA seq data. From the list of genes that were generated from the RNAseq data, the majority have not been characterised and therefore it has been difficult to establish a connection between them and *lama1* or how they would be affected from the developmental issues that arise in the *lama1*^{nl14} mutants. Moreover, except for *clusterin,* none of the genes have been shown to be expressed or linked to the eye. *Clusterin,* which is known to be a regulator of neuronal cell death and localizes to the extracellular matrix (Jeong et al., 2014), shows an increased expression in the lens thus opening the possibility that *lama1*^{nl14} has an increased number of dying cells in the lens.

This was surprising as we had not seen a lens phenotype as we did in *lama1*^{nl15} or with other characterised alleles.

Not only is there an increase in *clusterin* expression in the lens of mutants but also in a high percentage of mutants the increased expression is asymmetric and may coincide with a monolateral coloboma. In the study that had tested *bal*^{tp82} by OKR they suggested that the vision loss in this allele was due to the dysmorphogenesis of the lens (Biehlmaier, Makhankov and Neuhauss, 2007). As a lens defect had not been observed by brightfield microscopy in the *lama1*^{nl14} allele, by performing a TUNEL assay we could confirm whether there is an increase in cell death in the lens and whether this is causing opacity or dysmorphogenesis to the lens. Therefore, this could be why the OKR data from the larvae with subtle coloboma show a slight decrease in vision loss, the stimulus is unable to penetrate the lens as well as in a wild-type sibling. Although given that the lens phenotype is mainly asymmetric, cell death doesn't explain the reduced visual performance in both *lama1*^{nl14} mutant eyes.

Moreover, the lens is in contact with the intraocular vasculature and therefore abnormalities in lens structure have also been associated with vascular abnormalities (Alvarez *et al.*, 2007). Given that *lama1*^{nl15} mutant have lens extrusion, it would be interesting to analyse the vasculature in this allele; if we are able to observe a more severe vasculature defect in *lama1*^{nl15} larvae it would support the hypothesis that the lens is an essential structure in the maturation of the hyaloid vasculature. To correlate a hypothetical increase in cell death to vision loss and potential problems in the vasculature, we would have to analyse lens and vasculature structures after performing the OKR test.

Despite the coloboma phenotype being subtle in *lama1*^{nl14} we did not expect to discover many significant differentially expressed genes, it is however surprising that we did not find any neural development genes of interest. Some of the *lama1*^{nl14} mutants display expansion of the ventral retina into the diencephalon and in some cases quite severely. However, this result may be due to how we selected our embryos for RNA seq. As the phenotype is not penetrant, selecting embryos was difficult, we had so few in the clutches and as the severe cases of coloboma are only a small percentage of the mutants,

it could be that they were diluted in the samples. To rectify this, we could alter the parameters of the RNA seq data and lower the threshold of significantly altered genes and investigate whether any linked genes become apparent.

4.7 Perspectives and Future Directions

From the data we have shown the *lama1* alleles are similar to those previously published and summarised in section 1.9. However, it will be necessary to perform some of these experiments in the *nl15* allele. We had originally avoided it due to the severity of the lens extrusion and the difficulty with imaging, however, we could select mutants where the lens dysmorphogenesis may not appear as severe and test if imaging would be manageable. This will be of great benefit to the ongoing studies, particularly in regard to the investigation linking *lama1* to hyaloid vasculature defects. It will be interesting to observe if there is the same delay in *nl15* as *nl14* or even, if there is a more severe vasculature defect as previously shown by Semina *et al.*, 2006.

Further, it will be interesting to perform the bodipi staining as shown in ***Figure 13C-D'*** in the *nl15* allele. Not only would we be able to visualise if this more severe allele displays ectopic localisation of photoreceptors as it does in the *a69* allele but to also get a better view of whether there is any disruption to the retinal lamination overall (Semina *et al.*, 2006).

Again, we will compare the severities of mis-guided retino-tectal projections by performing DiI/DiO labelling in *nl15*. However, due to the severity of the notochord and body axis phenotypes we are not able to perform OKR on these larvae.

With regards to *nl14*, it will be necessary to perform the TEM at a time point where we know the coloboma phenotype is strong. We will therefore be able to do a direct comparison to a wild-type and understand the ultra-structural differences between a coloboma mutant and a wild-type sibling. Additionally, we will be able to investigate the morphology of the photoreceptors and determine if there is a shortening of the outer segment which we had initially thought was possible. With TEM, we will also be able to understand if there

are any disruptions to the basement membrane surrounding the lens and through the choroid fissure to confirm laminins importance in these structures and its role in the lens and coloboma phenotypes.

Moreover, we will perform time lapse imaging, focusing on optic cup morphogenesis. This will be to compare the development of the optic cup in the *nl14* and *nl15* alleles to determine if there is any structural defect in these mutants. Moreover, in understanding if there is any structural issue in these mutants, we could rule out an additional cause of vision loss in the OKR experiment.

5 Conclusion

In this study we have identified *lama1* as an additional candidate gene involved in choroid fissure fusion and coloboma. We have found that *lama1*^{nl14} show several differences with the previously studied *lama1* alleles. Despite *lama1*^{nl14} being a milder allele of *lama1* and presenting a very subtle coloboma, vision is compromised in these mutants. The causes of vision loss in *lama1*^{nl14} mutants are at least in part due to retino-tectal projection defects. The mechanism by which vision is decreased in *lama1*^{nl14} mutant eyes with no overt coloboma phenotype and retino-tectal projection defects should be followed up.

lama1^{nl14} mutants are an excellent sensitized background tool for addressing the role of extracellular matrix in eye morphogenesis and choroid fissure fusion.

6 References

Adler, R. and Canto-Soler, M. V. (2007) 'Molecular mechanisms of optic vesicle development: complexities, ambiguities and controversies.', *Developmental biology*, 305(1), pp. 1–13. doi: 10.1016/j.ydbio.2007.01.045.

ALSomiry, A. S., Gregory-Evans, C. Y. and Gregory-Evans, K. (2019) 'An update on the genetics of ocular coloboma', *Human Genetics*. doi: 10.1007/s00439-019-02019-3.

Alvarez, Y. *et al.* (2007) 'Genetic determinants of hyaloid and retinal vasculature in zebrafish'. doi: 10.1186/1471-213X-7-114.

Bazin-Lopez, N. *et al.* (2015) 'Watching eyes take shape', *Current Opinion in Genetics and Development*. Elsevier Ltd, pp. 73–79. doi: 10.1016/j.gde.2015.02.004.

Beck, J. C. *et al.* (2004) 'Quantifying the ontogeny of optokinetic and vestibuloocular behaviors in zebrafish, medaka, and goldfish.', *Journal of neurophysiology*, 92(6), pp. 3546–61. doi: 10.1152/jn.00311.2004.

Bernstein, C. S. *et al.* (2018) 'The cellular bases of choroid fissure formation and closure.', *Developmental biology*, 440(2), pp. 137–151. doi: 10.1016/j.ydbio.2018.05.010.

Bibliowicz, J., Tittle, Rachel K. and Gross, J. M. (2011) 'Toward a Better Understanding of Human Eye Disease', in. doi: 10.1016/b978-0-12-384878-9.00007-8.

Bibliowicz, J., Tittle, Rachel K and Gross, J. M. (2011) 'Toward a better understanding of human eye disease insights from the zebrafish, Danio rerio.', *Progress in molecular biology and translational science*, 100, pp. 287–330. doi: 10.1016/B978-0-12-384878-9.00007-8.

Biehlmaier, O., Makhankov, Y. and Neuhauss, S. C. F. (2007) 'Impaired retinal differentiation and maintenance in zebrafish laminin mutants.', *Investigative ophthalmology & visual science*, 48(6), pp. 2887–94. doi: 10.1167/iovs.06-1212.

de Bruijn, E., Cuppen, E. and Feitsma, H. (2009) 'Highly Efficient ENU Mutagenesis in Zebrafish.', *Methods in molecular biology (Clifton, N.J.)*, 546, pp. 3–12. doi: 10.1007/978-1-60327-977-2_1.

Bryan, C. D., Chien, C.-B. and Kwan, K. M. (2016) 'Loss of laminin alpha 1 results in multiple structural defects and divergent effects on adhesion during vertebrate optic cup morphogenesis.', *Developmental biology*, 416(2), pp. 324–37. doi: 10.1016/j.ydbio.2016.06.025.

Buono, L. *et al.* (2020) 'Analysis of gene network bifurcation during optic cup morphogenesis in zebrafish', *bioRxiv*. Cold Spring Harbor Laboratory, p. 2020.05.28.121038. doi: 10.1101/2020.05.28.121038.

Canto-Soler, M. V. and Adler, R. (2006) 'Optic cup and lens development requires Pax6 expression in the early optic vesicle during a narrow time window.', *Developmental biology*, 294(1), pp. 119–32. doi: 10.1016/j.ydbio.2006.02.033.

Cao, M. *et al.* (2018) 'Metalloproteinase adamts16 is required for proper closure of the optic fissure', *Investigative Ophthalmology and Visual Science*. doi: 10.1167/iovs.17-22827.

Carrara, N. *et al.* (2019) 'Temporal characterization of optic fissure basement membrane composition suggests nidogen may be an initial target of remodeling', *Developmental*

Biology. Academic Press, 452(1), pp. 43–54. doi: 10.1016/J.YDBIO.2019.04.012.

Cavodeassi, F. (2018) 'Dynamic Tissue Rearrangements during Vertebrate Eye Morphogenesis: Insights from Fish Models', *Journal of Developmental Biology*, 6(1), p. 4. doi: 10.3390/jdb6010004.

Cavodeassi, F. and Wilson, S. W. (2019) 'Looking to the future of zebrafish as a model to understand the genetic basis of eye disease.', *Human genetics*, 138(8–9), pp. 993–1000. doi: 10.1007/s00439-019-02055-z.

Cechmanek, P. B. and McFarlane, S. (2017) 'Retinal pigment epithelium expansion around the neural retina occurs in two separate phases with distinct mechanisms', *Developmental Dynamics*. doi: 10.1002/dvdy.24525.

Chhetri, J., Jacobson, G. and Gueven, N. (2014) 'Zebrafish-on the move towards ophthalmological research', *Eye (Basingstoke)*. Nature Publishing Group, pp. 367–380. doi: 10.1038/eye.2014.19.

Chow, R. L. and Lang, R. A. (2001) 'Early eye development in vertebrates.', *Annual review of cell and developmental biology*, 17, pp. 255–96. doi: 10.1146/annurev.cellbio.17.1.255.

clusterin (no date). Available at: https://zfin.org/ZDB-GENE-040426-1774.

Culverwell, J. and Karlstrom, R. O. (2002) 'Making the connection: retinal axon guidance in the zebrafish The retinotectal system in developmental biology', *CELL & DEVELOPMENTAL BIOLOGY*, 13, pp. 497–506. doi: 10.1016/S1084-9521(02)00103-9.

Dhakal, S. *et al.* (2015) 'Abnormal retinal development in Cloche mutant zebrafish', *Developmental Dynamics*. doi: 10.1002/dvdy.24322.

Eckert, P. *et al.* (2017) 'Optic fissure margin morphogenesis sets the stage for consecutive optic fissure fusion, pioneered by a distinct subset of margin cells using a hyaloid vessel as scaffold', *bioRxiv*. Cold Spring Harbor Laboratory, p. 141275. doi: 10.1101/141275.

Edwards, M. M. and Lefebvre, O. (2013) 'Laminins and retinal vascular development', *Cell Adhesion & Migration*, 7(1), pp. 82–89. doi: 10.4161/cam.22480.

Erskine, L. and Herreral, E. (2015) 'Connecting the retina to the brain', *ASN Neuro*. doi: 10.1177/1759091414562107.

Fadool, J. M. and Dowling, J. E. (2008) 'Zebrafish: A model system for the study of eye genetics', *Progress in Retinal and Eye Research*. doi: 10.1016/j.preteyeres.2007.08.002.

Fuhrmann, S. (2010) *Eye morphogenesis and patterning of the optic vesicle*, *Current Topics in Developmental Biology*. doi: 10.1016/B978-0-12-385044-7.00003-5.

Gestri, G. *et al.* (2018) 'Cell Behaviors during Closure of the Choroid Fissure in the Developing Eye.', *Frontiers in cellular neuroscience*, 12, p. 42. doi: 10.3389/fncel.2018.00042.

Gestri, G., Link, B. A. and Neuhauss, S. C. F. (2012) 'The visual system of zebrafish and its use to model human ocular Diseases', *Developmental Neurobiology*. doi: 10.1002/dneu.20919.

Goldberg, M. F. (1997) 'Persistent fetal vasculature (PFV): An integrated interpretation of signs and symptoms associated with persistent hyperplastic primary vitreous (PHPV) LIV Edward Jackson Memorial Lecture', in *American Journal of Ophthalmology*. Elsevier Inc., pp. 587–626. doi: 10.1016/S0002-9394(14)70899-2.

Gregory-Evans, C. Y. *et al.* (2004) 'Ocular coloboma: A reassessment in the age of molecular neuroscience', *Journal of Medical Genetics*, pp. 881–891. doi: 10.1136/jmg.2004.025494.

Hardy, H. *et al.* (2019) 'Detailed analysis of chick optic fissure closure reveals Netrin-1 as an essential mediator of epithelial fusion', *eLife*. eLife Sciences Publications, Ltd, 8. doi: 10.7554/elife.43877.

Hartsock, A. *et al.* (2014) 'In vivo analysis of hyaloid vasculature morphogenesis in zebrafish: A role for the lens in maturation and maintenance of the hyaloid', *Developmental Biology*. Academic Press Inc., 394(2), pp. 327–339. doi: 10.1016/j.ydbio.2014.07.024.

Heermann, S. *et al.* (2015) 'Eye morphogenesis driven by epithelial flow into the optic cup facilitated by modulation of bone morphogenetic protein', *eLife*. eLife Sciences Publications Ltd, 2015(4). doi: 10.7554/eLife.05216.

Hehr, C. L., Halabi, R. and McFarlane, S. (2018) 'Polarity and morphogenesis of the eye epithelium requires the adhesion junction associated adaptor protein Traf4.', *Cell adhesion & migration*, 12(5), pp. 489–502. doi: 10.1080/19336918.2018.1477900.

Henriques, P. M. *et al.* (2019) 'Nucleus Isthmi Is Required to Sustain Target Pursuit during Visually Guided Prey-Catching', *Current Biology*. Cell Press, 29(11), pp. 1771-1786.e5. doi: 10.1016/j.cub.2019.04.064.

Hero, I. (1989) 'The optic fissure in the normal and microphthalmic mouse', *Experimental Eye Research*. doi: 10.1016/0014-4835(89)90093-6.

Huang, Y.-Y. and Neuhauss, S. C. F. (2008) 'Swiss Federal Institute of Technology (ETH) Zurich, Department of Biology,Zurich, Switzerland, University of Zurich, Winterthurerstrasse 190, CH-8057 Zurich, Switzerland 2 Institute of Zoology', *Technology*.

Hug, N., Longman, D. and Cáceres, J. F. (2015) 'Mechanism and regulation of the nonsense-mediated decay pathway', *Nucleic Acids Research*. Oxford University Press, pp. 1483–1495. doi: 10.1093/nar/gkw010.

Ivanovitch, K., Cavodeassi, F. and Wilson, S. W. (2013) 'Precocious acquisition of neuroepithelial character in the eye field underlies the onset of eye morphogenesis.', *Developmental cell*, 27(3), pp. 293–305. doi: 10.1016/j.devcel.2013.09.023.

James, A. *et al.* (2016) 'The hyaloid vasculature facilitates basement membrane breakdown during choroid fissure closure in the zebrafish eye.', *Developmental biology*, 419(2), pp. 262–272. doi: 10.1016/j.ydbio.2016.09.008.

Jeong, Y.-M. *et al.* (2014) 'Induction of clusterin expression by neuronal cell death in Zebrafish.', *Journal of genetics and genomics = Yi chuan xue bao*, 41(11), pp. 583–9. doi: 10.1016/j.jgg.2014.08.007.

Karlstrom, R. O. *et al.* (1996) 'Zebrafish mutations affecting retinotectal axon pathfinding.', *Development (Cambridge, England)*.

Kaufman, R. *et al.* (2015) 'Development and origins of Zebrafish ocular vasculature', *BMC Developmental Biology*. doi: 10.1186/s12861-015-0066-9.

Kitambi, S. S. *et al.* (2009) 'Small molecule screen for compounds that affect vascular development in the zebrafish retina', *Mechanisms of Development*. Elsevier, 126(5–6), pp. 464–477. doi: 10.1016/J.MOD.2009.01.002.

Kwan, K. M. *et al.* (2012) 'A complex choreography of cell movements shapes the vertebrate eye', *Development*. Development, 139(2), pp. 359–372. doi:

10.1242/dev.071407.

Kwan, K. M. (2014) 'Coming into focus: The role of extracellular matrix in vertebrate optic cup morphogenesis', *Developmental Dynamics*. doi: 10.1002/dvdy.24162.

Lee, J. and Gross, J. M. (2007) 'Laminin β1 and γ1 containing laminins are essential for basement membrane integrity in the zebrafish eye', *Investigative Ophthalmology and Visual Science*. doi: 10.1167/iovs.06-1211.

Li, Z., Joseph, N. M. and Easter, S. S. (2000) 'The morphogenesis of the zebrafish eye, including a fate map of the optic vesicle', *Developmental Dynamics*, 218(1), pp. 175–188. doi: 10.1002/(SICI)1097-0177(200005)218:1<175::AID-DVDY15>3.0.CO;2-K.

Liu, C. *et al.* (2016) 'A secreted WNT-ligand-binding domain of FZD5 generated by a frameshift mutation causes autosomal dominant coloboma', *Human Molecular Genetics*. Oxford University Press, 25(7), pp. 1382–1391. doi: 10.1093/hmg/ddw020.

Long, K. R. and Huttner, W. B. (2019) 'How the extracellular matrix shapes neural development.', *Open biology*, 9(1), p. 180216. doi: 10.1098/rsob.180216.

Lupo, G., Harris, W. A. and Lewis, K. E. (2006) 'Mechanisms of ventral patterning in the vertebrate nervous system', *Nature Reviews Neuroscience*, pp. 103–114. doi: 10.1038/nrn1843.

Malicki, J. *et al.* (2016) 'Analysis of the retina in the zebrafish model.', *Methods in cell biology*, 134, pp. 257–334. doi: 10.1016/bs.mcb.2016.04.017.

Martin-Belmonte, F. and Mostov, K. (2008) 'Regulation of cell polarity during epithelial morphogenesis.', *Current opinion in cell biology*, 20(2), pp. 227–34. doi: 10.1016/j.ceb.2008.01.001.

Martinez-Morales, J. R. *et al.* (2009) 'Ojoplano-mediated basal constriction is essential for optic cup morphogenesis', *Development*. The Company of Biologists Ltd, 136(13), pp. 2165–2175. doi: 10.1242/dev.033563.

Martínez-Morales, J. R., Rodrigo, I. and Bovolenta, P. (2004) 'Eye development: a view from the retina pigmented epithelium.', *BioEssays : news and reviews in molecular, cellular and developmental biology*, 26(7), pp. 766–77. doi: 10.1002/bies.20064.

Martinez-Morales, J. R. and Wittbrodt, J. (2009) 'Shaping the vertebrate eye.', *Current opinion in genetics & development*, 19(5), pp. 511–7. doi: 10.1016/j.gde.2009.08.003.

Minevich, G. *et al.* (2012) 'CloudMap: A cloud-based pipeline for analysis of mutant genome sequences', *Genetics*, 192(4), pp. 1249–1269. doi: 10.1534/genetics.112.144204.

Molday, R. S. and Moritz, O. L. (2015) 'Photoreceptors at a glance', *Journal of Cell Science*. doi: 10.1242/jcs.175687.

Moreno-Marmol, T., Cavodeassi, F. and Bovolenta, P. (2018) 'Setting Eyes on the Retinal Pigment Epithelium', *Frontiers in Cell and Developmental Biology*. doi: 10.3389/fcell.2018.00145.

Morris, A. C. (2011) 'The genetics of ocular disorders: insights from the zebrafish.', *Birth defects research. Part C, Embryo today : reviews*, 93(3), pp. 215–28. doi: 10.1002/bdrc.20211.

Mueller, K. P. and Neuhauss, S. C. F. (2010) 'Quantitative measurements of the optokinetic response in adult fish', *Journal of Neuroscience Methods*, 186(1), pp. 29–34. doi:

10.1016/j.jneumeth.2009.10.020.

Nicolá S-Pé Rez, M. *et al.* (2016) 'Analysis of cellular behavior and cytoskeletal dynamics reveal a constriction mechanism driving optic cup morphogenesis'. doi: 10.7554/eLife.15797.001.

Patel, A. and Sowden, J. C. (2019) 'Genes and pathways in optic fissure closure', *Seminars in Cell and Developmental Biology*. doi: 10.1016/j.semcdb.2017.10.010.

Pathania, M., Semina, E. V and Duncan, M. K. (2014) 'Lens extrusion from Laminin alpha 1 mutant zebrafish.', *TheScientificWorldJournal*, 2014, p. 524929. doi: 10.1155/2014/524929.

Paulus, J. D. and Halloran, M. C. (2006) 'Zebrafish bashful/laminin-α1 mutants exhibit multiple axon guidance defects', *Developmental Dynamics*. Dev Dyn, 235(1), pp. 213–224. doi: 10.1002/dvdy.20604.

Petros, T. J., Rebsam, A. and Mason, C. A. (2008) 'Retinal axon growth at the optic chiasm: to cross or not to cross.', *Annual review of neuroscience*, 31, pp. 295–315. doi: 10.1146/annurev.neuro.31.060407.125609.

Randlett, O., Norden, C. and Harris, W. A. (2011) 'The vertebrate retina: a model for neuronal polarization in vivo.', *Developmental neurobiology*, 71(6), pp. 567–83. doi: 10.1002/dneu.20841.

Richardson, R. *et al.* (2016) 'The zebrafish eye—a paradigm for investigating human ocular genetics Zebrafish as a model organism', *Nature Publishing Group*. doi: 10.1038/eye.2016.198.

Richardson, R. *et al.* (2019) 'Transcriptome profiling of zebrafish optic fissure fusion', *Scientific Reports*. doi: 10.1038/s41598-018-38379-5.

Rinner, O., Rick, J. M. and Neuhauss, S. C. F. (2005) 'Contrast sensitivity, spatial and temporal tuning of the larval zebrafish optokinetic response', *Investigative Ophthalmology and Visual Science*. doi: 10.1167/iovs.04-0682.

Semina, E. V *et al.* (2006) 'Mutations in laminin alpha 1 result in complex, lens-independent ocular phenotypes in zebrafish'. doi: 10.1016/j.ydbio.2006.07.005.

Seth, A. *et al.* (2006) 'Belladona/(lhx2) is required for neural patterning and midline axon guidance in the zebrafish forebrain', *Development*, 133(4), pp. 725–735. doi: 10.1242/dev.02244.

Sidhaye, J. and Norden, C. (2017) 'Concerted action of neuroepithelial basal shrinkage and active epithelial migration ensures efficient optic cup morphogenesis', *eLife*. eLife Sciences Publications Ltd, 6. doi: 10.7554/eLife.22689.

Sinn, R. and Wittbrodt, J. (2013) 'An eye on eye development', *Mechanisms of Development*. doi: 10.1016/j.mod.2013.05.001.

Varshney, S., Hunter, D. D. and Brunken, W. J. (2015) 'Extracellular Matrix components regulate cellular polarity and tissue structure in the developing and mature Retina', *Journal of Ophthalmic and Vision Research*. doi: 10.4103/2008-322X.170354.

Vihtelic, T. S. *et al.* (2001) 'Arrested differentiation and epithelial cell degeneration in zebrafish lens mutants', *Developmental Dynamics*. Dev Dyn, 222(4), pp. 625–636. doi: 10.1002/dvdy.1217.

Voss, J. and Bischof, H.-J. (2009) 'Eye movements of laterally eyed birds are not

independent.', *The Journal of experimental biology*, 212(Pt 10), pp. 1568–75. doi: 10.1242/jeb.024950.

Weiss, O. *et al.* (2012) 'Abnormal vasculature interferes with optic fissure closure in lmo2 mutant zebrafish embryos', *Developmental Biology*. Academic Press, 369(2), pp. 191–198. doi: 10.1016/J.YDBIO.2012.06.029.

Williams, S. E., Mason, C. A. and Herrera, E. (2004) 'The optic chiasm as a midline choice point', *Current Opinion in Neurobiology*. doi: 10.1016/j.conb.2004.01.010.

Williamson, Kathleen A and FitzPatrick, D. R. (2014) 'The genetic architecture of microphthalmia, anophthalmia and coloboma.', *European journal of medical genetics*, 57(8), pp. 369–80. doi: 10.1016/j.ejmg.2014.05.002.

Williamson, Kathleen A. and FitzPatrick, D. R. (2014) 'The genetic architecture of microphthalmia, anophthalmia and coloboma', *European Journal of Medical Genetics*. Elsevier Masson SAS, 57(8), pp. 369–380. doi: 10.1016/j.ejmg.2014.05.002.

Wilson, S. W. and Houart, C. (2004) 'Early steps in the development of the forebrain.', *Developmental cell*, 6(2), pp. 167–81. Available at: http://www.ncbi.nlm.nih.gov/pubmed/14960272 (Accessed: 24 July 2019).

Young, R. M. *et al.* (2019) 'Compensatory growth renders Tcf7l1a dispensable for eye formation despite its requirement in eye field specification', *eLife*. eLife Sciences Publications Ltd, 8. doi: 10.7554/eLife.40093.

Zhao, C., Wang, Q. and Temple, S. (2017) 'Stem cell therapies for retinal diseases: Recapitulating development to replace degenerated cells', *Development (Cambridge)*. Company of Biologists Ltd, pp. 1368–1381. doi: 10.1242/dev.133108.

Zinkevich, N. S. *et al.* (2006) 'laminin alpha 1 gene is essential for normal lens development in zebrafish', *BMC Developmental Biology*. doi: 10.1186/1471-213X-6-13.

Zolessi, F. R. *et al.* (2006) 'Polarization and orientation of retinal ganglion cells in vivo.', *Neural development*, 1, p. 2. doi: 10.1186/1749-8104-1-2.

Zuber, M. E. *et al.* (2003) 'Specification of the vertebrate eye by a network of eye field transcription factors.', *Development (Cambridge, England)*, 130(21), pp. 5155–67. doi: 10.1242/dev.00723.